Improving the stability of CeO_2 catalyst by rare earth metal promotion and molecular insights in the dimethyl carbonate synthesis from CO_2 and methanol with 2-cyanopyridine

Dragos Stoian[†, ‡, §], Francisco Medina[‡], Atsushi Urakawa[*†]

[†] Institute of Chemical Research of Catalonia (ICIQ), The Barcelona Institute of Science and Technology, Av. Països Catalans 16, 43007 Tarragona, Spain

[‡] Department of Chemical Engineering, University Rovira i Virgili, Av. Països Catalans 26, 43007 Tarragona, Spain

*Email: aurakawa@iciq.es

Abstract

The unmatched efficiency of the direct dimethyl carbonate (DMC) synthesis from CO_2 and methanol over CeO_2 catalysts in the presence of an organic dehydrating agent (2-cyanopyridine, 2-CP) was recently reported with high DMC yield (>90%) in both batch and continuous operations. However, the CeO_2 catalyst gradually deactivates in the time-scale of days due to suggested surface poisoning by 2-picolinamide (2-PA) produced by hydration of 2-CP. This work seeks for active and stable CeO_2-based catalysts and aims to understand the material factors influencing the catalytic performance. Surface modification of CeO_2 by the addition of rare earth metal (REM) was found effective to improve the catalyst stability. Surface basicity and reducibility of the Ce^{4+} species play important roles in preventing catalyst deactivation by stabilizing the reactive methoxy species in comparison to the poisoning species (2-PA or species alike). This has been evidenced by *in situ* ATR-IR spectroscopy. CeO_2 materials promoted with 1 wt% rare earth metals (La, Gd, and Pr) greatly enhanced the catalyst stability while retaining the high catalytic activity of CeO_2. Among them, 1 wt% Pr promotion to CeO_2 was the most effective, affording 35% higher DMC yield in comparison to bare CeO_2 after 150 h time on stream under the optimized reaction condition of 30 bar and 120 °C.

Keywords: carbon dioxide, methanol, dimethyl carbonate, cerium oxide, 2-cyanopyridine, rare earth metal, surface properties, *in situ* ATR-IR.

1. Introduction

One of the major global challenges urged by the climate change and the desired paradigm shift from the fossil-fuels dependent society to a more sustainable one is the carbon management, i.e. how to efficiently utilize carbon dioxide (CO_2) being emitted and accumulated in the atmosphere. Catalytic transformation of CO_2 into useful chemicals such as organic and inorganic carbonates via non-reductive CO_2 transformations has been widely investigated for that aim.[1-3] Among others, the synthesis of alkyl carbonates through direct carboxylation reaction of alcohols like methanol (**Reaction 1**, synthesis of dimethyl carbonate (DMC)) is very attractive in terms of atom economy.[1, 4]

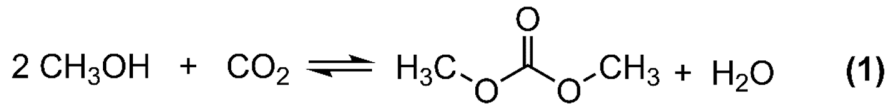

DMC is a versatile chemical and represents an ecologically benign alternative to toxic and corrosive methylating or carbonylating agents such as methyl halides (CH_3X), dimethyl sulfate (DMS), and phosgene ($COCl_2$).[1, 4-7] DMC is used in the synthesis of polycarbonates and polyurethanes, as solvent replacing methyl ethyl ketone, butanone, and *tert*-butyl acetate, and as electrolyte in lithium ion batteries.[1-2, 4] Furthermore, DMC has gained wide attention as an oxygenate fuel additive due to its high oxygen content, thus increasing combustion performance.[8]

In the methanol carboxylation reaction with CO_2, many heterogeneous catalysts have been investigated to date. ZrO_2, SiO_2, Al_2O_3, TiO_2, H-ZSM5, H-USY, H-MOR, ZnO, MoO_3, Bi_2O_3, MgO, Y_2O_3, HfO_2, La_2O_3, Pr_6O_{11}, Ga_2O_3, GeO_2, In_2O_3, Sb_2O_3, and hybrid ones (e.g. H_3PO_4/V_2O_5 and Cu-Ni/V_2O_5-SiO_2) have been tested, but without or with very low

activity (e.g. 0.3 mmol DMC g_{cat}^{-1} h^{-1} for zirconia (ZrO_2) materials).[9-13] Occasionally, dimethyl ether (DME) instead of DMC was produced via dehydration reaction of methanol, which is commonly catalyzed by acidic sites, especially at elevated temperatures (>150 °C). According to previous studies, ZrO_2 and ceria (CeO_2) are the unique materials effectively catalyzing the DMC formation.[9-10, 14-21] However, the major challenge is associated with the thermodynamics of **Reaction 1**, which is generally unfavorable due to equilibrium limitation. Even under thermodynamically favorable high-pressure conditions (ca. 400 bar), DMC yield is ca. 1% in accordance with the thermodynamic expectation.[22-24] Therefore, it is imperative to employ an effective mean to shift the equilibrium to the product side for potential commercialization of DMC synthesis from CO_2 and methanol. It is well known that water removal can shift the equilibrium improving DMC yield. Chemical (e.g. 2, 2-dimethoxy propane) or physical water traps[17, 25] and catalytic membrane reactors[26] have been employed for this purpose, but the improvement had been relatively minor.

In 2013, Tomishige *et al.* described the DMC synthesis over CeO_2 in a batch reactor using a nitrile (2-cyanopyridine, 2-CP) as an organic dehydrating agent and reported an exceptionally high DMC yield of 94%. In the reaction, CeO_2 functioned as an effective catalyst for both DMC synthesis and nitrile hydrolysis, forming the corresponding amide (2-picolinamide, 2-PA, **Reaction 2**).[27-28]

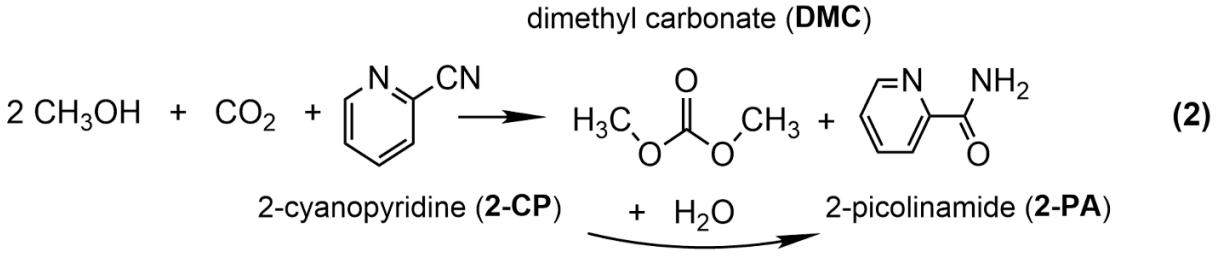

(2)

They also verified the recyclability of 2-PA by dehydrating 2-PA back to 2-CP with Na_2O/SiO_2 as catalyst. Together with the formation of DMC and 2-PA, very small amounts of methyl picolinate (Me-PCN) and methyl carbamate (Me-CBM) were found as byproducts. Me-PCN is co-produced with NH_3 arising from the reaction between 2-PA and methanol, while Me-CBM originates from the reaction between DMC and NH_3 (**Scheme S1**, Supporting Information).

Inspired by the work of Tomishige *et al.*, our group reported continuous DMC synthesis over CeO_2 in a fixed-bed reactor in the presence of 2-CP under low-to-high pressure conditions (up to 300 bar).[24] Although striking DMC yields >90% were achieved during the continuous operation above 30 bar, a severe catalyst deactivation was noticed, resulting in more than 50% drop in methanol conversion in 10 days with a small loss (8-9%) in DMC selectivity. Our following investigation allowed unravelling the cause of the catalyst deactivation by visual and spectroscopic inspections using an optically transparent fused quartz reactor. Most importantly, results showed molecularly adsorbed 2-PA over the deactivated CeO_2 catalyst. However, the catalyst could be reactivated when the adsorbed 2-PA was removed from the surface by a simple thermal treatment in air at 300 °C which is close to the boiling point of 2-PA (284.1 °C).[29]

Motivated by the previous results and the superior DMC yield in the presence of 2-CP in comparison to other dehydrating agents[17, 30-31] using CeO_2 as catalyst, the present study seeks for stable and active CeO_2-based catalyst in the reaction under continuous operation as well as to understand material factors influencing the catalytic performance. The uniquely high catalytic activity of CeO_2 in this reaction may originate from the redox capabilities of the cerium oxide in conjunction with its acid-base properties[32-36]. Therefore,

in this work common strategies to modify the chemical properties (acidity/basicity) of CeO_2 by the addition of metal/metal oxides to CeO_2 to influence the oxygen storage capacity, defect stability, and mobility of oxygen atoms were examined and their impacts on catalyst stability were thoroughly investigated. Particularly, the effects of La,[37-39] Gd,[40-41] and Pr[42-45] promoters were investigated in depth to influence the oxygen defects/mobility of CeO_2 based materials while mildly altering the acid/base properties. Besides the use of an ordinary stainless-steel tubular reactor, an optically transparent fused-quartz tubular reactor was employed in order to visually assess the deactivating state of the catalysts under the optimized reaction conditions (30 bar and 120 °C).[29] The catalysts before and after the reactions were characterized by several techniques to identify critical material factors determining the catalytic activity and stability of the materials. Furthermore, molecular insights into the surface adsorbed active species responsible for the reaction and deactivation were gained by *in situ* attenuated total reflection (ATR)-IR spectroscopy, elucidating the nature of surface poisoning process and how REM promotion prevents it.

2. Experimental

2.1. Materials

High surface area powder of CeO_2 was kindly supplied by Daiichi Kigenso Kagaku Kogyo Co. Ltd., Japan and used without any further treatment. The CeO_2 material is nano-sized (high surface area) but highly crystalline, fulfilling the important requisites as active catalyst for the target reaction as reported by Tomishige *et al.* and for some CeO_2 materials such materials states can be effectively obtained after calcination at 600 °C.[19, 27] Rare earth metals (REM) promoted ceria materials (**x** wt% **M** on CeO_2, where **x** = 0.25,

1, and 5 and **M** = La, Gd, and Pr) were synthesized by the incipient wetness impregnation of the pristine CeO_2 with an aqueous solution of the metal precursor (lanthanum (III) nitrate hexahydrate, gadolinium (III) nitrate hydrate, and praseodymium (III) nitrate hydrate, respectively). The metal nitrates (99.9% purity) were purchased from Alfa Aesar. The impregnated materials were dried overnight at 80-90 °C in an oven and calcined at 400 °C for 4 h in a static air after a temperature ramp of 2 °C min^{-1}. Methanol (≥99.9%, HPLC grade) and 2-cyanopyridine (2-CP, 99%) were purchased from Sigma Aldrich. High purity CO_2 gas (>99.9993%) was purchased from Abelló Linde, Spain.

2.2. Reaction system

The details of the reaction set-up and analytical method for the identification and quantification of reaction products were described in our previous works.[24, 29] In a typical experiment, 300 mg of the catalyst (pelletized, crushed, and sieved to 200-300 μm particle size) was loaded into the reactor tube (a stainless-steel tube with ID: 1.74 mm and OD: 3.17 mm). For the visual inspection experiments, a fused quartz reactor (ID: 2.0 mm and OD: 3.0 mm) was used.[29] The CO_2 flow rate was kept at 6 NmL min^{-1}. The mixture of methanol and 2-CP at 2:1 molar ratio (methanol:CO_2 = 1:2.5, molar ratio) was passed to the reactor at 10 μL min^{-1} by means of an HPLC pump (Jasco, PU-2080 Plus).

All catalytic tests were performed under optimized reaction conditions where the DMC yield is high while the reaction pressure is relatively mild (30 bar and 120 °C).[29] We aimed to perform the reaction for over 100 h, but occasionally the reaction had to be stopped before due to the sealing issue of back pressure regulator (Jasco, BP-2080 Plus) caused by the high-temperature kept at the regulator and the clogging or damage of the sealing

materials.[29] Nevertheless, the reaction was performed more than 48 h to observe a clear trend in catalytic activity, evaluate catalyst deactivation, and calculate its rate.

2.3. Characterization

X-ray diffraction (XRD) measurements were made using a Siemens D5000 diffractometer (Bragg-Brentano parafocusing geometry and vertical θ-θ goniometer) fitted with a curved graphite diffracted-beam monochromator, incident and diffracted-beam Soller slits, a 0.06° receiving slit and scintillation counter as a detector. The angular 2θ diffraction range was between 5 and 70°. The data were collected with an angular step of 0.05° at 9 s per step (which resulted in a scan rate of 1°/3 min) and sample rotation with Cu-Kα radiation at 40 kV and 30 mA.

Temperature programmed desorption (TPD) experiments were performed using a Thermo Scientific™ TPDRO 1100 Advanced Catalyst Characterization System equipped with a flow-through quartz reactor and a thermal conductivity detector with a tungsten filament. In a typical experiment a catalyst material (100-150 mg) was firstly subjected to the following pretreatments, (i) drying / thermal treatment under He at 400 / 600 °C for 1 h, (ii) CO_2 (4% CO_2 in He) / NH_3 (5% NH_3 in He) saturation at 80 °C for 30 min, and (iii) flushing under He at 80 °C for 30 min. A TPD experiment consisted of ramping the temperature from room temperature to 800 °C at a ramp of 10 °C min^{-1} under He flow at 20 mL min^{-1}. The effluent gases were analyzed by a mass spectrometer (Pfeiffer Omnistar GSD 301 C). An anhydrous magnesium perchlorate ($Mg(ClO_4)_2$) trap was used for CO_2-

TPD experiments to absorb mainly H_2O, whereas no trap was used for NH_3-TPD experiments.

Temperature programmed reduction experiments with hydrogen (H_2-TPR), were performed using the same apparatus as in the TPD experiments. 50-70 mg of a sample was first pretreated at 100 °C for 1 h under N_2 stream and subsequently heated from 50 to 800 °C at the ramp rate of 5 °C min^{-1} under the flow of 5% H_2 in N_2 at 20 ml min^{-1}. A soda lime ($CaO + Na_2O$) trap was used to remove H_2O and CO_2.

The textural properties (BET surface area and BJH pore size distribution) of the materials were determined by N_2 physisorption experiments using Quantachrome Instruments, AUTOSORB iQ. The material (100-150 mg) was firstly outgassed at 150 °C at 4 mbar to clean the sample surface and pores prior to the measurements.

In situ ATR-IR measurements (ZnSe crystal, multiple reflections) were performed using a PIKE HATR accessory on a Bruker Tensor 27 spectrometer equipped with a LN-MCT detector at 4 cm^{-1} resolution. An aqueous slurry containing catalyst particles was deposited via drop-casting method over the ZnSe crystal at room temperature and dried. The reaction cell was then closed and the temperature was increased to 120 °C. The catalyst was kept for 2-3 h under a flow of inert (N_2). The measurements were performed with the N_2 flow saturated with methanol or methanol+2-CP mixture (15 mmol 2-CP in methanol) at room temperature. For all the experiments the gas flow rate was 10 NmL min^{-1}.

Ex situ Raman measurements were carried out on a Thermo Scientific™ Nicolet™ iS™50 FT-IR spectrometer equipped with 1064 nm near-infrared excitation laser. The instrument

was preferably used to avoid the strong fluorescence shown by the samples after the catalytic test with 532/785 nm laser.[29] *Ex situ* Raman measurements (for fresh materials) were carried out on a BWTEK dispersive i-Raman spectrometer equipped with 532 nm excitation laser and a TE-cooled linear array detector.

FT-IR measurements of the samples before and after the reaction were performed on a Bruker Alpha spectrometer equipped with a DTGS detector at 2 cm^{-1} resolution in an ATR sampling configuration with a diamond internal reflection element.

Thermogravimetric analysis (TGA) of the samples before and after the reaction was performed on a Mettler Toledo TGA/SDTA 851 equipment. In a typical experiment, 3-5 mg of a catalyst placed in an alumina crucible were subjected to heating from 25 to 800 °C at a ramp rate of 5 °C min^{-1} under a flow of synthetic air at 50 mL min^{-1}.

3. Results and discussion

3.1. Effects of rare earth metal promotion

We have thoroughly examined the effects of surface modifications by REM addition on the stability of CeO_2 catalyst during the DMC synthesis and on the physicochemical properties of the catalyst materials. Different approaches to improve the stability, such as Ce-Zr solid-solutions and precious metals (PM) promoted CeO_2 (i.e. 1 wt% Rh, Ru, and Pd) were also studied but these approaches were not effective in improving the stability; rather they suppressed the catalytic activity of CeO_2. Therefore, these results are described in detail only in Supporting Information.

Figure 1a depicts the effects of La addition to CeO_2 (0.25, 1, and 5 wt% La) on the long-term stability of the catalytic activity (methanol conversion, X_{MeOH} and DMC selectivity,

S_{DMC}) in the continuous DMC synthesis. Initially, slightly lower X_{MeOH} values (ca. 88%) were detected for all La-promoted CeO_2 materials as compared to that of the bare CeO_2 (92.5%), but all La-containing catalysts performed better than CeO_2 after 60 h. About 74% X_{MeOH} was observed for 0.25 wt% La-CeO_2 at 71 h and 5 wt% La-CeO_2 showed ca. 75% X_{MeOH} at 86 h of the reaction. Remarkably, the most stable catalyst within the La-series was 1 wt% La-CeO_2 which maintained a high activity (>80% of X_{MeOH}) even at 120 h, in contrast to ca. 60% X_{MeOH} with CeO_2 at the same time on stream. The La addition also impacted on the DMC selectivity. Initially, the higher the La loading, the poorer the S_{DMC} (>99% for bare CeO_2 and ca. 85% for the 5 wt% sample). The S_{DMC} values leveled off with time to ca. 92-93% and the most stable sample, 1 wt% La-CeO_2, displayed 94% S_{DMC} at 120 h of reaction.

The effects of Gd addition (0.25, 1, and 5 wt% Gd) to CeO_2 on the long-term reactivity are compared in **Figure 1b**. 0.25 and 1 wt% Gd catalysts exhibited a higher level of initial X_{MeOH} compared to the La-promoted catalysts and at the same level as that of CeO_2. However, further increase of Gd loading to 5 wt% lowered the initial X_{MeOH} to 87%. Importantly, all the Gd-containing catalysts displayed better long-term stability than CeO_2. 81-82% X_{MeOH} was observed for 0.25 and 5 wt% Gd-CeO_2 at 68 and 50 h of the reaction, respectively. Similarly to the case of the La-promoted CeO_2, the most stable catalyst was 1 wt% Gd-CeO_2 which maintained a very high activity (84% X_{MeOH}) even at 100 h of the reaction, which is significant considering 63% X_{MeOH} using CeO_2 at 100 h. Furthermore, Gd addition resulted in high and stable S_{DMC} (mostly >98%) at all loadings over the reaction time tested. Based on the superior stability of the catalytic activity at high S_{DMC}, 1 wt% was found to be the optimal Gd loading for the DMC synthesis.

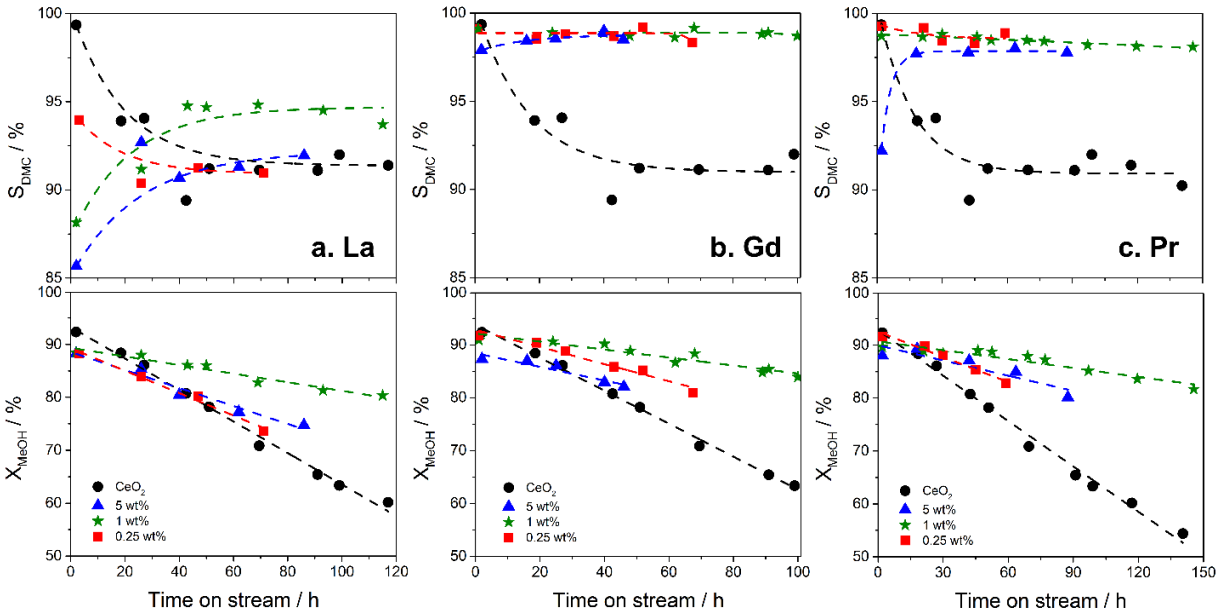

Figure 1. Effects of REM promoters on the stability of methanol conversion (X_{MeOH}, lower panels) and DMC selectivity (S_{DMC}, upper panels) in the DMC synthesis from CO_2 and methanol in the presence of 2-CP at 120 °C, 30 bar for **a.** La-CeO_2 (left panels), **b.** Gd-CeO_2 (middle panels), and **c.** Pr-CeO_2 (right panels). Different symbols are used to distinguish the data points of catalyst materials as follows: black circles - bare CeO_2, red squares – 0.25 wt% REM, green stars – 1 wt% REM, and blue triangles – 5 wt% REM. The dashed lines represent the trend lines to guide eyes for S_{DMC} and to calculate deactivation rates of X_{MeOH} (**Figure 2**) with a linear fitting.

Furthermore, the effect of Pr addition (0.25, 1, and 5 wt% Pr) to CeO_2 on the reactivity was investigated (**Figure 1c**). The initial X_{MeOH} slightly decreased more notably at increased Pr loading, i.e. 92% (0.25 wt%), 90% (1 wt%), and 88% (5 wt%). However, similar to Ga-promoted catalysts, X_{MeOH} for all Pr-promoted catalysts became higher than that of CeO_2 after ca. 30 h due to the higher long-term stability. 83% X_{MeOH} was observed for 0.25 wt% Pr-CeO_2 at 60 h, while 5 wt% Pr-CeO_2 showed 80% X_{MeOH} at 88 h. As in the case of the other REM addition, the most stable catalyst was once again confirmed to be at 1 wt% loading. The catalyst could maintain remarkable 82% X_{MeOH} in comparison to 50% observed for CeO_2 at 150 h. Moreover, Pr addition showed similarly stable S_{DMC} as

observed for the Gd-promoted catalysts. 0.25 and 1 wt% Pr catalysts were highly selective to DMC (>98% at ca. 150 h of the reaction for the 1 wt% sample), whereas 5 wt% Pr catalyst showed comparably lower S_{DMC}, especially during the initial phase.

The above study of REM (La, Gd, Pr) promotion to CeO_2 clearly shows its positive impacts, leading to higher stability in both activity (X_{MeOH}) and DMC selectivity, thus significantly improving the overall performance. When 1 wt% Pr-CeO_2 and CeO_2 are compared, an increase of around 35% in the DMC yield for the Pr-promoted catalyst was obtained at ca. 150 h, which is significant and of high relevance in practice.

Figure 2 summarizes the results on the catalyst stability in terms of deactivation rate, expressed by the drop in X_{MeOH} (%) per hour. Since the deactivation was reasonably linear for all REM-promoted samples (**Figure 1**), the slope was calculated with the least squares method assuming a linear trend line of X_{MeOH}. Obviously, the incorporation of REM was positive in terms of long-term catalytic activity and the positive effects were more evident for Gd- and Pr-CeO_2. As noted above, the best materials were 1 wt% REM catalysts, showing the lowest rate of deactivation (0.080, 0.075, and 0.055 % h^{-1} for La-, Gd-, and Pr-CeO_2 respectively) in comparison to 0.253 % h^{-1} of CeO_2. In addition, it should be reminded that 1 wt% Gd- and Pr-promoted catalysts were the best materials in terms of long term stability in S_{DMC}. When the REM loading is higher (at 5 wt%), the catalytic activity is lowered due to more influential effects of pure REM oxides (e.g. La and Pr) which show intrinsically lower catalytic activity compared to CeO_2 for the hydration of 2-CP to 2-PA.[46]

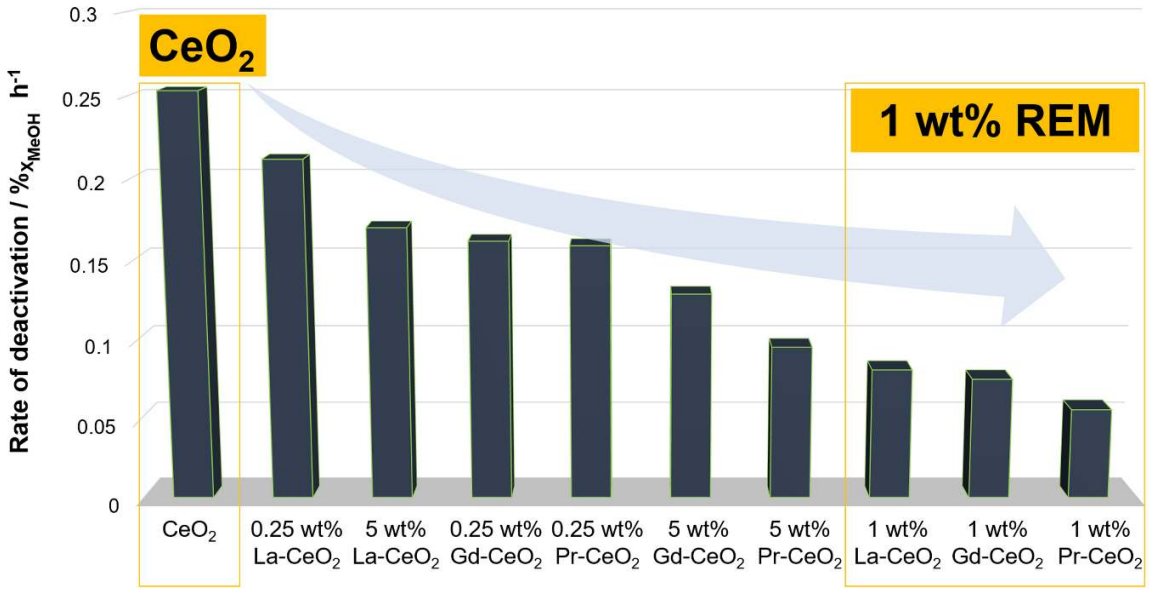

Figure 2. Rate of deactivation during the DMC synthesis (120 °C, 30 bar) expressed by the drop in X_{MeOH} (%) per hour for pristine CeO_2 and REM-promoted CeO_2 materials.

3.2. Characterization of pristine and as-synthesized catalysts

The stability studies presented in **section 3.1** showed the positive effects of REM as promoter of CeO_2 in the DMC synthesis in the presence of 2-CP, especially at 1 wt% loading. In order to identify the origin of the enhanced stability of the REM-promoted catalysts, the chemical and structural properties of the pristine and as-synthesized catalysts as well as spent catalysts were investigated in detail.

Structural and textural properties

The XRD patterns of the pristine CeO_2 and as-synthesized materials incorporating REM are presented in **Figure S2** (Supporting Information). CeO_2 showed the peaks corresponding to (111), (200), (220), and (311) planes of cubic fluorite phase. The materials with REM showed negligible structural changes, indicating that metal promoters were finely dispersed on the surface of CeO_2.

The BET surface area and pore volume of all materials are presented in **Table S1** (Supporting Information). Addition of REM to CeO_2 consistently decreased the surface area (the higher the loading, the lower the surface area), while the materials containing 5 wt% REM showed a clear reduction in the pore volume. Importantly, the changes in the textural properties and bulk structure of the materials are not correlated with the catalytic activity and stability.

Raman investigation

To elucidate the effects of REM addition on the CeO_2 structure, the materials were further characterized by Raman spectroscopy (**Figure S3**). The results suggest that the REMs are atomically incorporated into CeO_2 judging from the absence of REM sesquioxide bands[47] near 400-420 cm^{-1}, corroborated with a minor shift and with an intensity change of the F_{2g} Raman active band of CeO_2 at ca. 460 cm^{-1}. Moreover, the characteristic band due to oxygen vacancies of CeO_2 at ca. 570 cm^{-1} emerges upon REM-doping.[48] This band is more pronounced at higher amount of doped REM. Among REM-CeO_2 materials, Pr-CeO_2 shows the highest intensity ratio of the bands at 570 and 460 cm^{-1} (I_{570}/I_{460}), commonly used as the measure of oxygen vacancies.[49] Another indication in this direction is the small band around 250 cm^{-1} which is more prominent for Pr-CeO_2. These features imply that in case of Pr-CeO_2, oxygen vacancies are located closer to the surface where catalysis takes place in comparison to La- and Gd-CeO_2. Therefore, it can be inferred that Pr is the best promoter to effectively modify the CeO_2 surface structure by its atomic-level dispersion, creating oxygen vacancies near the surface. Also 5 wt% Pr addition likely leads to over-modification and the loss of active CeO_2 surface required for the reaction due to intrinsically lower activity of PrO_2 compared to CeO_2.[46] Creation of oxygen

vacancies on CeO_2 can lead to the creation of a unique surface state which enhances the surface exposed Ce atoms and improves the stability of the catalyst as discussed later.

Basicity and acidity of the catalysts

As mentioned in **Introduction**, several acid-base heterogeneous catalysts have been tested in the direct carboxylation of methanol with CO_2. While the basic sites are generally required to activate CO_2 molecule, both acidic and basic sites are often reported to be mandatory for methanol activation (CH_3O^- and CH_3^+ formation). It has been widely reported that ZrO_2, CeO_2, and CeO_2–ZrO_2 solid solution show both acidic and basic characters.[50] CeO_2 possesses Lewis acidic (Ce^{4+}) and basic (O^{2-}) sites and the material may have exactly the right acidity-basicity balance to catalyze the reaction, more precisely the two reactions of DMC synthesis and hydration reaction of 2-CP.[27-28] Besides the acid-base property, the unique feature of the CeO_2 material compared to many other oxides is the reducibility of the catalyst and lattice/surface oxygen mobility. It is not yet clear but the latter features may play pivotal roles in DMC synthesis and related to the catalyst stability. Similarly, it has been previously suggested that addition of Cu in low amount (0.1 to 0.5 wt%) may work cooperatively with CeO_2 catalysts to accelerate the partial reduction of Ce^{4+} sites to Ce^{3+}, enhancing the DMC yield by 20-60%.[51] For these reasons, acidity and basicity characterization by NH_3- and CO_2-TPD and material reducibility by H_2-TPR were performed to evaluate possible correlations between material properties and catalytic performance.

According to Hutter *et al.* [52] who investigated the adsorption mechanism of CO_2 on CeO_2 (111) by DFT calculations, three stable configurations of CO_2 on the CeO_2 surface have been identified: (i) monodentate carbonate, (ii) bidentate carbonate, and (iii) linearly adsorbed species. Among these three configurations, the linear species are represented as a physically adsorbed CO_2 (no hybridization of orbitals of the linear CO_2) and the monodentate species are the most stably adsorbed ones. On the other hand, both mono- and bi-dentate carbonate species are represented by bent CO_2 configurations having the C atom chemically bonded to O atom on the surface. The stronger the interaction of CO_2 with the CeO_2 surface, the higher its desorption temperature, i.e. the low (20-200 °C), medium (200-450 °C), and high temperature (>450 °C) desorption peaks are assigned to linear, bidentate and monodentate carbonates, respectively.[53] In the same manner, the low (20-200 °C), medium (200-450 °C), and high temperature (>450 °C) desorption peaks in NH_3-TPD measurements will be attributed to the weak, medium, and strong acid sites, respectively.

CO_2- and NH_3-TPD profiles of all catalysts are presented in **Figure S4** in Supporting Information and the amounts of adsorbed-desorbed CO_2 and NH_3 are summarized in **Table S2** (Supporting Information), respectively. Generally, the addition of a foreign atom on/in the CeO_2 structure reduced the amount of adsorbed CO_2/NH_3 and thus the total number of acidic and basic sites. In other words, the bare CeO_2 material is more acidic and more basic compared to the doped/promoted CeO_2 materials, judging from the number of the sites. There were clear and consistent trends in the changes of acidity and basicity by the addition of REM to CeO_2 (**Figure S4 B**). In all cases, the total number of acidic and basic sites became smaller, and the degree of the decrease was less at lower

REM loading without affecting the characteristics of the strength of acidity and basicity, as evident from the similar desorption profiles of CO_2- and NH_3-TPD for the 0.25 wt% REM-CeO_2 to those of CeO_2. Upon increasing the REM loading to 1 and 5 wt%, there were notable changes in the nature of the strong acidic and basic sites with the formation of two types of strong basic sites (desorption at ca. 500 and 700 °C). For acidic sites, mildly strong sites (desorption at ca. 500 °C) were reduced but strong sites (at ca. 750 °C) were enhanced. Thus, it can be concluded that higher loading of REM reduces the number of weak-moderate acidic/basic sites but increases that of strong acidic/basic sites.

With the aim to identify the role of acidity, basicity and their synergy in the reaction, we evaluated the relations between acidity, basicity, or a unifying parameter (i.e. basicity/acidity ratio calculated from the total amount of the adsorbed probe molecules) of the examined materials and their catalytic performance and stability. When the basicity/acidity ratio is larger than 1 (i.e. more basic catalysts; CeO_2 and REM-promoted CeO_2), all the materials display good catalytic activity at the initial phase of the reaction. In contrast, when the basicity/acidity ratio is <1 (i.e. more acidic) the materials such as CeO_2-ZrO_2 solid solutions, ZrO_2 and PM-CeO_2 series exhibited lower activity (**Figure 3**). It is widely reported that DMC synthesis from CO_2 and methanol requires the presence of both acidic and basic sites.[10] This study comes as a confirmation to that statement as well as an indication of the importance of a proper balance between acidity and basicity of catalyst. Weak acidity is important in the selective DMC synthesis since the formation of common by-product, dimethyl ether (DME), is more easily catalyzed over strong acid sites, especially at higher temperatures.[54] Moreover, 2-PA (weak base) adsorption over

the acidic sites of CeO_2 leads to a severe catalyst deactivation.[29] Importantly, basicity seems playing more important roles by activating the CO_2 molecule and formation of CH_3O^- species and monodentate methyl carbonate (MMC, CH_3OCOO-metal atom) as possible reaction intermediates.[9, 19, 55] The relatively high basicity of CeO_2 against its acidity is mildly influenced by the addition of REM unlike the materials with comparably lower basicity when Zr and PM are added (**Table S2**, Supporting Information). This basicity/acidity ratio is thus a good indicator to evaluate the activation capability of catalyst for the reaction and it should be higher than the threshold (in our case >1).

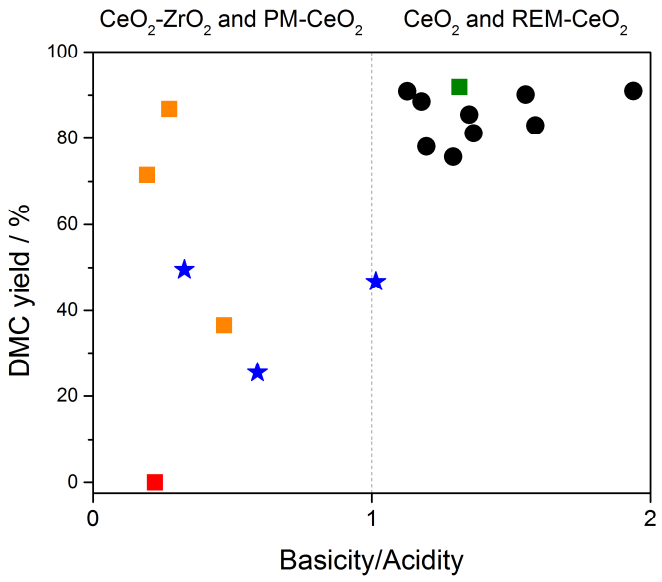

Figure 3. Initial DMC yield against basicity/acidity ratio for all examined materials of this study at 120 °C, 30 bar. Different symbols are used to distinguish the data points of catalyst materials as follows: squares for pure CeO_2 (green), pure ZrO_2 (red) and CeO_2-ZrO_2 solid solutions (orange), blue stars for PM-CeO_2, and the black circles for REM-CeO_2. The data points can be extracted from **Figure S4**/**Table S2**.

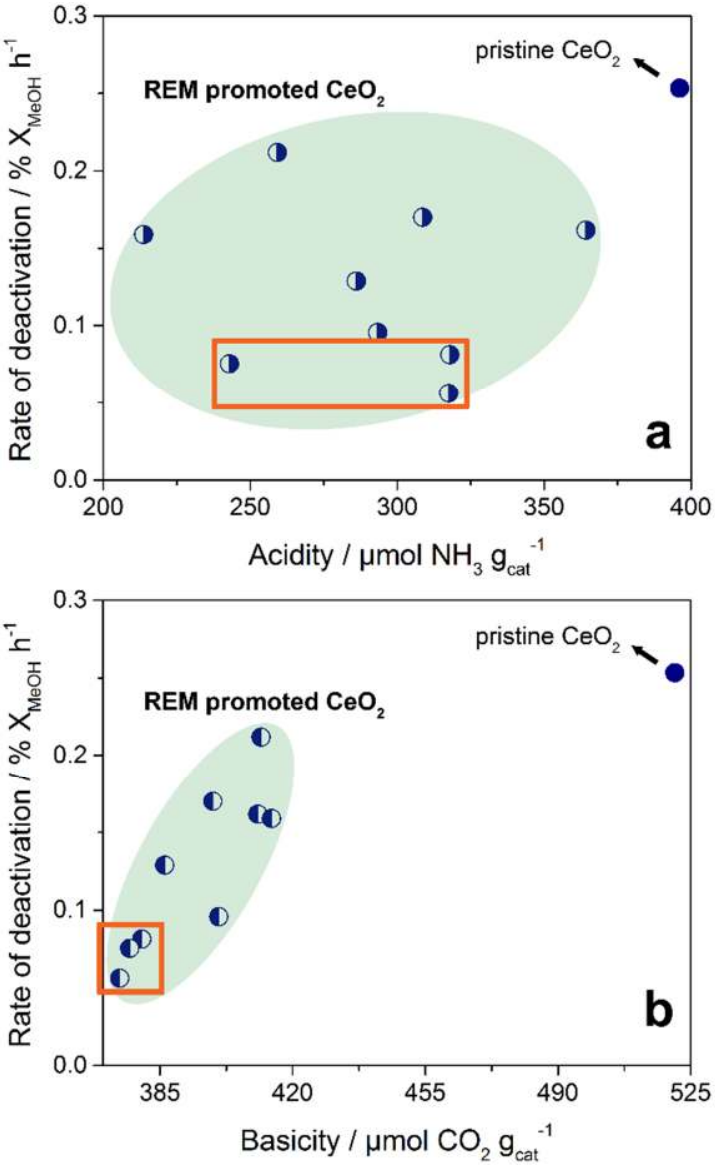

Figure 4. Rate of deactivation in the DMC synthesis plotted against (a) acidity and (b) basicity of CeO_2 and REM-CeO_2 materials. Filled circles are for pristine CeO_2, while the half-empty circles correspond to the REM promoted CeO_2. The orange rectangles mark the values for the 1 wt% REM promoted materials.

Furthermore, possible correlations of the rate of deactivation with the parameters related to acidity or basicity were sought for the promising REM-promoted materials. **Figure 4** presents the rate of deactivation for CeO_2 and REM-CeO_2 as a function of the basicity and acidity expressed by the total number of sites determined by the CO_2- and NH_3-TPD

experiments. Albeit no clear correlation was found for the deactivation rate with acidity, the influence of the basicity on the deactivation was consistent; the lower the basicity, the lower the rate of deactivation. This implies that basicity likely induces the surface poisoning and thus deactivation, which is rather non-intuitive due to the expected stronger interaction of 2-PA with acidic sites. This point will be discussed in detail later with the identification and quantitative analysis of surface adsorbed species during the reaction.

Reducibility of the catalysts

The reducibility of the CeO_2-based catalysts reflected by the oxygen mobility[56-58] were studied by H_2-TPR. The H_2-TPR profiles of pristine CeO_2 and REM-promoted CeO_2 are presented in **Figure S5** and **Figure S6** (Supporting Information), respectively. **Figure 5** presents a comparison of the profiles for the best performing materials (1 wt% REM-CeO_2) and pristine CeO_2. **Table S3** (Supporting Information) summarizes the H_2 uptake of all the samples investigated.

The reduction of CeO_2 is known to proceed in two steps; the first one at ca. 500 °C, corresponding to the reduction of surface Ce (IV) atoms more relevant for the catalytic processes, and the second one at ca. 800 °C, corresponding to the bulk reduction of the material (elimination of O^{2-} from the lattice and formation of Ce_2O_3).[34, 58-59] The reducibility of ceria is known to be strongly dependent on the CeO_2 crystallite size.[33, 60] The CeO_2 used in this study has a high surface area with a crystallite size of ca. 10 nm (as calculated from the Scherrer equation using the (111) reflection peak) and it presents clearly the two major peaks assignable to surface reduction (peak at 487 °C) and bulk reduction (peak at 816 °C) processes (**Figure S5**).

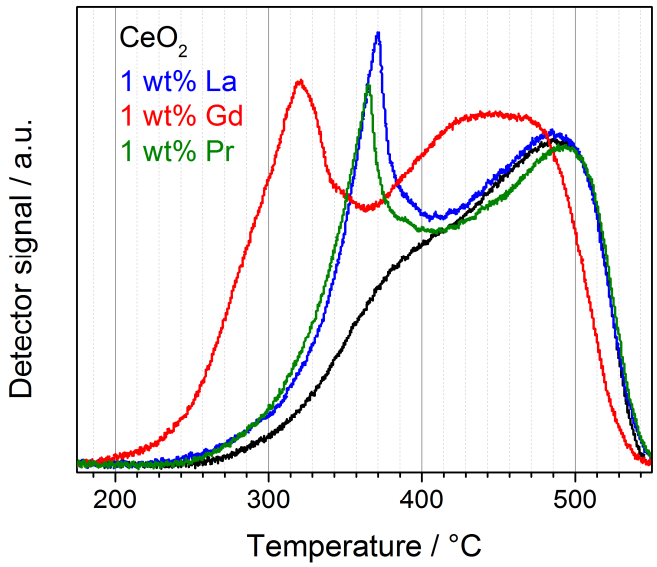

Figure 5. H_2-TPR profiles (corresponding to the surface reduction region) for CeO_2 and 1 wt% REM-CeO_2 materials.

Clear and consistent changes in the material reducibility were observed for the REM promoted CeO_2 materials (**Figure S6**). At 0.25 wt% REM loading, the changes in reducibility were not pronounced. At 1 and 5 wt% REM loading, the appearance of highly reducible features of the materials was evident with a new shoulder-peak at ca. 310-380 °C for all REM types (5 wt% La displayed two shoulders). Interestingly, the presence of such a shoulder-peak near the low temperature CeO_2 reduction has been attributed to the existence of Ce^{4+} located in different chemical environment, such as the subsurface region.[61-63] Even more importantly, in the case of the catalysts with high stability in the reaction (i.e. 1 wt% REM loading) the surface reduction peak was shifted to slightly lower temperatures as compared to the case of CeO_2 (**Figure 5**), reported previously due to the enhanced redox property of CeO_2, for example by the function of Pr.[64] Precisely, the low temperature peak which started to rise at 235 °C for CeO_2 shifted to lower reduction-onset temperature of 210, 170, and 220 °C for 1 wt% La-, Gd-, and Pr-CeO_2, respectively.

Among 5 wt% REM-CeO_2 materials, only the La-CeO_2 showed the same behavior reducing the onset temperature of surface reduction at ca. 160 °C, whereas for Gd- and Pr-CeO_2 showed higher onset temperature compared to the corresponding 1 wt% REM-CeO_2. Also, it is worth noting that 0.25 and 1 wt% REM loading did not affect considerably the shape of the surface reduction peak, while at 5 wt% REM loading, the materials displayed a small decrease of the peak. This is in a good agreement with the textural properties where increasing the REM loading to 5 wt% resulted in a decrease of ca. 25% in the S_{BET}, indicating less CeO_2 available on the surface.

In summary, at 1 wt% REM loading the reducibility of CeO_2 is enhanced while retaining the good reducibility of surface CeO_2 which may be responsible for the catalytic activity. On the other hand, at 0.25 wt% REM loading does not sufficiently influence material properties determining the catalytic activity (i.e. acid-base properties and reducibility), while 5 wt% REM loading leads to an over-enhanced basicity and diminished active surface area (notable loss in surface area and pore volume) besides intrinsic lower activity of REM oxides compared to CeO_2.[46]

3.3. Characterization of pristine and 1 wt% REM-CeO_2 before and after the reaction

The long-term stability of CeO_2 catalyst in the direct DMC synthesis in the presence of 2-CP was markedly improved using REM promoters (i.e. La, Gd, and Pr), but there was still a gradual and substantial deactivation of the catalyst materials over more than 100 h of reaction. To better understand and explain the effects of the REM promoters and their functions during the reaction, bare CeO_2 and 1 wt% REM-CeO_2 after the reaction were characterized by visual, spectroscopic and thermal analyses. The reactions (120 °C, 30

bar, for 30 h) were performed in a fused quartz reactor to enable visual inspection and Raman spectroscopy of the materials within the reactor. Prior to the analyses, the catalysts were thoroughly washed with methanol at 120 °C at 3 mL min^{-1} for 15 min in the reactor to remove the crystallites of 2-PA deposited over the catalyst surface, accordingly to our previous study.[29] This washing procedure is necessary to identify strongly adsorbed surface molecular species causing catalyst deactivation by Raman and ATR-IR spectroscopic studies.[29]

Visual inspection and spectroscopic investigation

Figure 6 shows the photographs of the catalysts before and after the reaction with subsequent hot methanol washing. Initially, all materials displayed a light-yellow color characteristic of pristine CeO_2 except Pr-CeO_2 in a reddish tint. After the reaction, all the materials turned darker and there seems a correlation between the degree of catalyst deactivation and the degree of the color change. This tendency is the most noticeable for CeO_2 turning into dark maroon and less color change was observed for 1 wt% La-CeO_2. Even less change in color was observed for 1 wt% Gd-CeO_2. 1 wt% Pr-CeO_2 changed its color to brick-red due to the reddish color of the as-synthesized material.

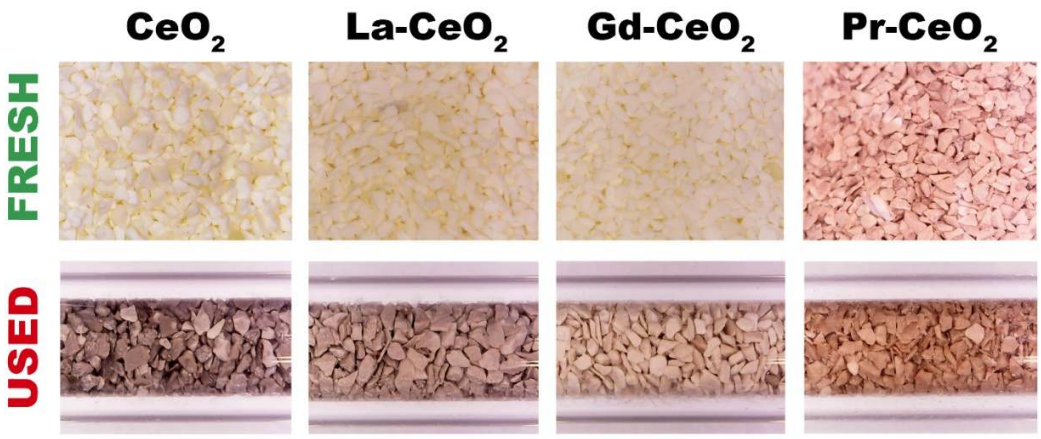

Figure 6. Photographs of CeO_2 and REM-CeO_2 materials before (top) and after (below) the reaction at 120 °C, 30 bar for 30 h and a subsequent hot methanol washing at 120 °C for 15 min.

Interestingly, the degree of the color changes was in good agreement with the changes in the surface area (S_{BET}) and pore volume of the materials after the reaction (**Table 1**). 32.5% S_{BET} loss was observed for CeO_2, while the La, Gd, and Pr promoted samples showed ca. 29% (La and Gd) and 24% (Pr) S_{BET} loss. Moreover, the decrease in the pore volume of the materials was perfectly in accordance with the rate of deactivation (**Figure 2**); CeO_2 losing 31.5% of its pore volume and La, Gd, and Pr samples losing 18.3%, 12.1%, and 9.2%, respectively. No structural change in the crystallinity of the materials was detected by XRD after 30 h of the reaction (**Figure S9**, Supporting Information).

Table 1. BET surface area and pore volume of CeO_2 and REM-CeO_2 before and after the reaction (120 °C, 30bar, for 30 h) and subsequent hot methanol washing at 120 °C.

Material	Surface area (m^2 g^{-1})		Decrease (%)	Pore volume (cm^3 g^{-1})		Decrease (%)
	Before	*After*		*Before*	*After*	
Pristine CeO_2	160	108	32.5	0.197	0.135	31.5
1 wt% La-CeO_2	135	97	28.1	0.186	0.152	18.3
1 wt% Gd-CeO_2	146	104	28.8	0.199	0.175	12.1
1 wt % Pr-CeO_2	139	106	23.7	0.184	0.167	9.2

Ex situ Raman and ATR-IR measurements were performed to clarify the cause of the catalyst deactivation by identifying the surface adsorbed species (**Figure S10**). Both Raman and IR studies indicate that 2-PA-like species (more precisely, 2-PA monoanion, Py-$CONH^-$) are adsorbed on the surfaces in accordance with our previous study of bare CeO_2 where band assignments are described,[29] implying that the REM promoters do not influence the adsorption mode and origin of deactivation. Based on the intensity of the Raman bands, the amount of 2-PA adsorbed on the surface of the pristine CeO_2 was suggested to be higher than that on the surface of REM-CeO_2 materials. This is in good agreement with the catalytic activity; catalyst deactivation is more pronounced when surface is more poisoned by a larger amount of adsorbed 2-PA. It is important to mention that the four materials re-gained their initial color and catalytic activity upon mild calcination treatment at 300 °C in air as demonstrated for CeO_2.[29]

TGA

Furthermore, thermogravimetric analysis (TGA) was performed for the catalyst materials before and after the reaction and the results are summarized in **Table 2** (TGA profiles are shown in **Figure S11**, Supporting Information). All the materials before the reaction showed only one desorption peak, assigned to the removal of surface impurities (i.e. physically adsorbed water). On the other hand, an additional feature of a peak slightly below 300 °C was observed for the materials after the reaction. This peak corresponds to the 2-PA elimination from the CeO_2 surface as the boiling point of 2-PA is 284.1 °C. It is interesting to note that the peak slightly shifts towards lower temperatures (ca. 270 °C) for 1 wt% REM-CeO_2 promoted materials as compared that of pristine CeO_2 (ca. 280 °C), as determined by peak calculation taking the first derivative of the weight loss curve. This is a good indication of weaker interaction between the 2-PA and the catalyst surface when CeO_2 is promoted with 1 wt% REM. The lower amount of 2-PA adsorption indicated by the Raman study was also confirmed by TGA (**Table 2**) where the REM promotion clearly reduced the degree of the weight loss for the catalysts after the reaction. These results agree with the changes of surface area and pore volume; the less 2-PA adsorbed, the less changes in the surface area and pore volume. REM promotion at the effective amount (1 wt%) leads to the reduction in basicity (**Figure 4**) and decreases the interaction between 2-PA and the catalyst surface. This results in reducing the rate of poisoning by 2-PA, thus enhancing the catalyst stability when 2-CP is used as dehydrating agent. When the basicity is sufficiently high compared to the acidity, the high activity of CeO_2 itself is retained also enhanced and become ideal for this reaction.

Table 2. Summary of TGA of the materials (CeO_2 and 1 wt% REM) before and after the reaction.

Material	Peak no.	Before reaction		After reaction	
		Weight loss / %	Peak max / °C	Weight loss / %	Peak max / °C
CeO_2	1	7.23	50.8	2.83	31.5
	2	-	-	5.21	277.5
1 wt% La-CeO_2	1	5.34	41	2.01	30.5
	2	-	-	4.64	272.9
1 wt% Gd-CeO_2	1	5.77	38.9	2.83	30.5
	2	-	-	3.59	268.5
1 wt% Pr-CeO_2	1	5.49	41.7	3.02	39.3
	2	-	-	3.39	268.5

Another important factor influencing the catalyst stability is the reducibility of the catalyst surface, which was promoted by REM, especially at 1 wt%, as discussed above. Redox properties change the charge state of atoms and this can consequently modulate the acid-base properties. When the reducibility is enhanced while retaining the active CeO_2 sites by REM (presumably those characterized by the H_2-TPR peak <500 °C), it is possible that the catalyst surface poisoned by 2-PA may change its redox state (Ce^{4+} ⇔ Ce^{3+}) flexibly under the reaction condition and create an environment facilitating 2-PA desorption from the surface. This hypothesis is supported by the lower desorption temperature of 2-PA in TGA for 1 wt% REM samples as discussed above. This would be naturally positive for the catalyst stability and it is speculated that 1 wt% Gd or Pr promotion is particularly effective in inducing such a function while retaining the active catalytic sites of CeO_2.

3.4. Understanding the deactivation mechanism: In situ ATR-IR studies

To gain deeper molecular insights into the deactivation mechanism and consequently the nature of active sites, we performed a series of *in situ* ATR-IR studies to identify the types of methoxy species formed over the catalyst surfaces and their relation to surface poisoning process by 2-PA or species alike. For comparison, we have studied chemical interactions of methanol and 2-CP with the surfaces of CeO_2 and 1 wt% Pr-CeO_2. **Figure 7** displays ATR-IR spectra obtained by alternatingly passing methanol vapor and N_2 over CeO_2 or Pr-CeO_2 at 120 °C. For both materials, as soon as the methanol vapor passes over the catalysts, the methoxy bands at ca. 1110 and 1060 cm^{-1} appeared and they gradually disappeared under N_2 flow accompanying redshifts which are indicative of stronger interaction of methoxy species with the surface at lower coverage. Marked differences were observed for the two catalysts in the absorbance, the relative ratio of the two bands, stability of the methoxy species under N_2 and band positions observed.

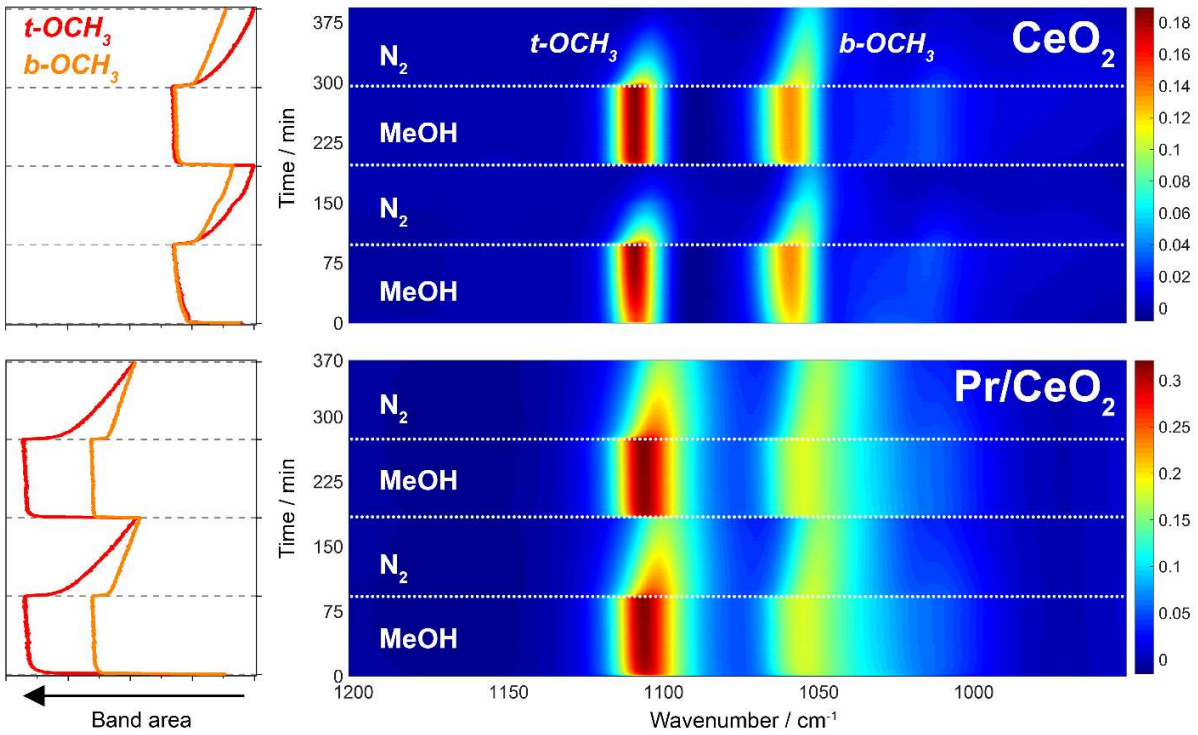

Figure 7. (right) *In situ* ATR-IR spectra of surface species formed by alternatingly passing methanol vapor in N_2 and N_2 over CeO_2 (top) and 1 wt% Pr-CeO_2 (bottom) at 120 °C. The background was taken in N_2 before admission of methanol. The scale is in absorbance. (left) The temporal evolution of the area of the two bands assigned to terminal methoxy (t-OCH_3, ca. 1110 cm^{-1}) and bridged methoxy (b-OCH_3, ca. 1060 cm^{-1}).

It is widely acknowledged that methanol can be easily dissociated on the acid−base sites of CeO_2 to form surface methoxy species (on the Lewis acid sites, Ce^{n+}) and proton (on the Lewis base sites, O^{2-}) even at room temperature.[65] The observed two bands can be unambiguously assigned to the C–O stretching modes of terminal (t-OCH_3, at ca. 1110 cm^{-1}) and bridged (b-OCH_3, ca. 1060 cm^{-1}) methoxy species.[19, 65] For the synthesis of DMC from CO_2 and methanol, t-OCH_3 was reported to play key roles since monomethyl carbonate (MMC, CH_3O-COO-), the suggested intermediate, can be formed by the

reaction between CO_2 and t-OCH_3.[19] On the other hand, the existence of b-OCH_3 species is related to the presence of oxygen defect sites on CeO_2.[66-68]

Figure 7 evidences higher amounts of adsorbed methoxy species of both types over Pr-promoted CeO_2. This may be closely related to the less number of basic sites as observed for 1wt% REM-CeO_2 (**Figure 4**), which can be interpreted as lower number of surface oxygen atoms of CeO_2 and thus consequently a higher number of surface exposed Ce atoms where the methoxy species can be formed. Interestingly, the temporal evolutions of the band areas of the two methoxy species (**Figure 7**) show that the ratios of t-OCH_3 to b-OCH_3 over the surface are different for the two catalysts. The Pr promotion enhanced the ratio of t-OCH_3 to b-OCH_3 from around 1 (CeO_2) to around 1.5 (Pr-CeO_2). Since defect sites are expected to enhance b-OCH_3, the enhanced relative population of t-OCH_3 observed for Pr-CeO_2 is counter-intuitive. A closer look into the spectral features (**Figure 7**) shows that the b-OCH_3 band on Pr-CeO_2 (1055 cm^{-1}) is redshifted and broadened in comparison to that on CeO_2 (ca. 1060 cm^{-1}). The broadness is indicative of the presence of various similar geometrical configurations of adsorbed methoxy species, thus of the existence of more defective adsorption sites over Pr-CeO_2. Pr can be directly involved in the enhanced interaction of methoxy with the surface as indicated by the redshift, but possibly methoxy species may be preferably adsorbed on the hollow Ce sites on Pr-CeO_2. The latter interpretation is consistent with the increased number of t-OCH_3 compared to b-OCH_3 observed for Pr-CeO_2, since involving more Ce atoms by hollow site adsorption (3 coordinating Ce atoms) than bridged site adsorption (2 coordinating Ce atoms) can lead to less b-OCH_3 species and thus increase t-OCH_3 population comparably.

Another important observation during this methanol sorption study is the stability of the methoxy species. Upon switching from methanol vapor to N_2 at the reaction temperature (120 °C), the number of surface methoxy species decreased, but to a different extent for the two materials. Within the duration of our experiments (N_2 flow for ca. 90 min), t-OCH_3 disappeared almost completely, whereas about 40% of b-OCH_3 (assuming the band area is proportional to the concentration of the methoxy species) remained on the bare CeO_2 after ca. 90 min of N_2 flow, clearly showing higher stability of b-OCH_3.[69] Strikingly, the stability of both methoxy species are greatly enhanced by Pr-promotion. The higher stability of b-OCH_3 compared to t-OCH_3 was also confirmed for Pr-CeO_2, showing even >70% of the b-OCH_3 present on the surface after ca. 90 min of N_2 flow at 120 °C.

To further clarify the importance of the enhanced stability of the methoxy species in terms of catalyst stability, we performed another *in situ* ATR-IR study by alternatingly passing a vapor containing 2-CP and methanol and that of methanol over the two materials at 120 °C to monitor surface chemical processes causing catalyst poisoning (**Figure 8**).

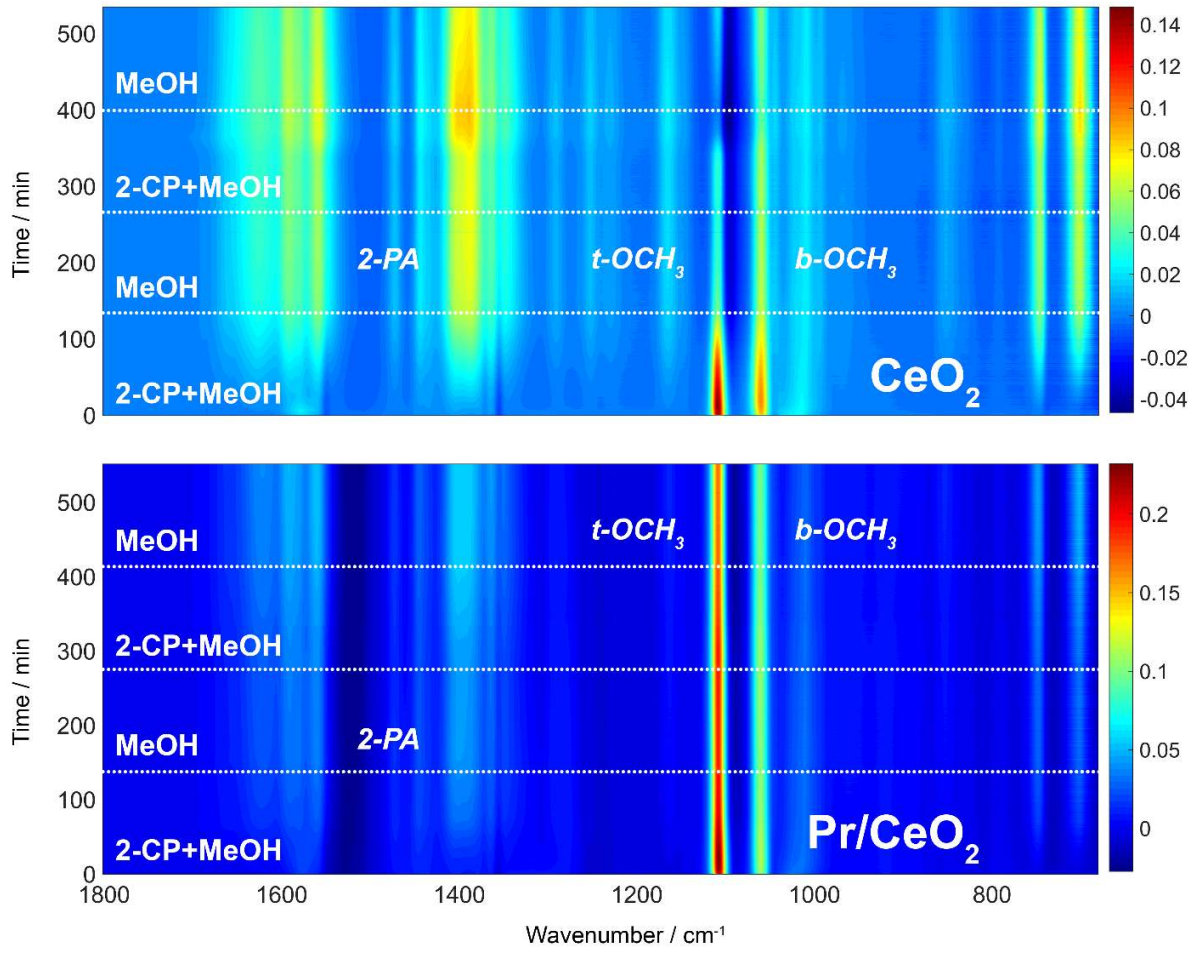

Figure 8. *In situ* ATR-IR spectra of surface species formed by alternatingly passing the vapor of methanol + 2-CP and that of methanol, both saturated in N_2, over CeO_2 (top) and 1 wt% Pr-CeO_2 (bottom) at 120 °C. The background was the material under N_2. The scale is in absorbance.

For CeO_2, as soon as the mixture of 2-CP and methanol passed over the catalysts the appearance of characteristic t-OCH_3 and b-OCH_3 bands at ca. 1110 and 1060 cm^{-1} was confirmed, followed by the gradual but significant decrease of the bands with time. This decrease of the methoxy bands accompanied the emergence of the bands characteristic of 2-PA anion (Py-$CONH^-$), assigned as 1560 cm^{-1} (δ_{NH}), 1390 cm^{-1} (ν_{C-N}) and 750 cm^{-1}

(δ_{ring}), as the surface intermediate in the hydrolysis of 2-CP towards 2-PA. Upon switching to methanol vapor as an attempt to "clean" the CeO_2 surface, the spectrum remained unaltered; the number of 2-PA-like species remained constant and the number of the methoxy species could not be recovered. Another admission of the vapor of 2-CP and methanol led to further decrease of the methoxy species and increase of the 2-PA-like species in exchange. Between the two methoxy species, the decrease of the band of t-OCH_3, which is suggested to be responsible for DMC formation, was more pronounced. It is interesting to note that this t-OCH_3 band could be recovered slightly by passing the vapor containing only methanol again, while b-OCH_3 band could not as much. These results prove that 2-PA-like species and methoxy species competitively adsorb on the same surface sites of CeO_2, thus causing surface poisoning by reducing the number of catalytically active methoxy species. The surface sites responsible for the formation of b-OCH_3 are more resistant to the poisoning likely due to the stronger adsorption strength of b-OCH_3 than t-OCH_3, while the recovery of the surface sites is difficult once they are poisoned.

The identical study with Pr-CeO_2 shows highly contrasting results with clear molecular insights into the REM promotion effects (**Figure 8**). As in the case of CeO_2, the 2-PA-like species were formed with time when the vapor of 2-CP and methanol was passed over Pr-CeO_2 but to a much lesser extent. Obviously, the stability of both methoxy species were greatly enhanced and thus made the surface highly resistant to the poisoning. Passing methanol vapor could not recover the surface methoxy species, indicating that when the sites are poisoned, the recovery is very difficult, in agreement with the slower but continuous decrease in the catalytic activity of the REM-promoted catalysts.

3.5. Active sites and deactivation mechanism

Based on the above studies, **Figure 9** summarizes mechanistic views on the active sites and deactivation of CeO_2 during the DMC synthesis from CO_2 and methanol in the presence of 2-CP. Methanol molecules adsorb over CeO_2 as t-OCH_3 and b-OCH_3 species (**Figure 9a**). When 2-CP reaches the surface, it is adsorbed as 2-PA like species (**Figure 9b**). A possible structure of adsorbed 2-CP over the defect site of CeO_2 was recently reported by Tamura *et al.*[65] and this state closely resembles the molecular structure of 2-PA and most likely this or the chemical state where N atom is hydrogenated/protonated is the state we have noted as 2-PA like species in this work. It is important to point out that this state of surface species can block both t-OCH_3 as well as b-OCH_3 sites. It was evidently shown that the surface sites of CeO_2 is competitively accessed by methanol and 2-CP. Over the surface of pure CeO_2, the 2-PA-like species are formed rapidly by occupying the sites capable of methoxy formation as shown spectroscopically (**Figure 8**). Since this 2-PA-like species hinders also the formation of t-OCH_3 species, thus the catalyst deactivates over time.

This study clearly demonstrated that REM-promotion could slow down the blocking of the active sites by 2-PA-like species by strengthening the adsorption of methoxy species, especially that of b-OCH_3 species. REM promoters enhanced the number of surface defects and sites allowing multiple coordination of Ce to stabilize the methoxy species. Also, the enhanced redox properties of REM-CeO_2 especially at 1 wt% REM loading seem optimum to achieve the most efficient stabilization of methoxy species while retaining sufficient number of t-OCH_3 sites for DMC synthesis. Besides, the enhanced oxygen mobility by REM may also slow down the formation of 2-PA-like species since the

oxygen defects in subsurface may facilitate conversion of the 2-PA-like species back to 2-CP.

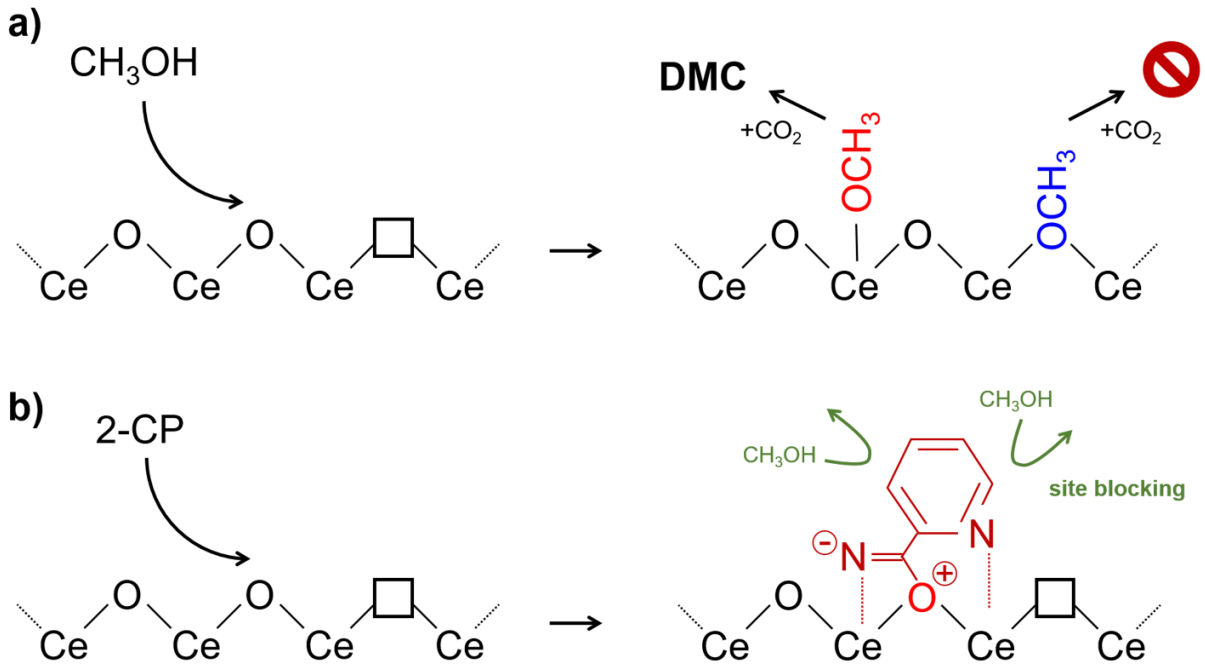

Figure 9. Simplified reaction scheme for DMC synthesis over CeO_2 in the presence of 2-CP. While DMC is formed by the reaction between CO_2 and t-OCH_3 (**a**), the adsorption of 2-CP and/or the subsequent hydrolysis step produces an intermediate (dark red) that leads to the poisoning of the methanol adsorption sites (**b**). Surface hydrogen atoms/protons are not shown for the sake of brevity.

4. Conclusions

Effects of different promoters to CeO_2 on the long-term behavior of catalytic performance in continuous DMC synthesis from CO_2 and methanol in the presence of a dehydrating agent (2-CP) were evaluated. Among them, 1 wt% rare earth metal (REM: La, Gd, or Pr)-promoted catalysts, especially Gd-CeO_2 and Pr-CeO_2, exhibited the highest stability without deteriorating the catalytic performance of pristine CeO_2. The visual, spectroscopic

(IR and Raman) and TGA investigations clarified that the surface adsorption of 2-PA produced by the hydration reaction of 2-CP is the cause of the catalyst deactivation and there was a clear relation between the amount of 2-PA adsorbed and the degree of catalyst deactivation. The origins of the promoter effects were studied in detail by characterizing the textural properties, acidity-basicity, and reducibility of the catalyst materials. The right balance in basicity and acidity, especially sufficiently high basicity/acidity ratio, is found necessary to achieve enhanced catalytic activity. The pure CeO_2 has the right acidity-basicity balance and this characteristic is retained for REM-promoted CeO_2 materials. Regarding the catalyst stability, when the number of basic sites is smaller and the catalyst reducibility is higher (i.e. easier to create surface defects and increased mobility of sub-surface O atoms to/from the CeO_2 surface), there were clear improvements. Remarkably, compared to CeO_2, 1 wt% Pr-CeO_2 and 1 wt% Gd-CeO_2 exhibited 35% higher DMC yield after 150 h and 25% higher DMC yield after 100 h of time on stream, respectively. This greatly enhanced catalyst stability by the REM promoters in the light of the previously found reactivation strategy (calcination at 300 °C in air) render the process more attractive in practice to produce DMC from CO_2 and methanol. Furthermore, molecular insights into the catalyst deactivation and thus the nature of active sites were uncovered by *in situ* ATR-IR spectroscopic studies. They clearly show that REM promoters enhance adsorption strength of methoxy species and thus prevents the 2-PA-like species from adsorbing and thus blocking the sites for DMC synthesis.

Acknowledgements

We thank the Generalitat de Catalunya for financial support through the CERCA Programme and recognition (2014 SGR 893) and MINECO (CTQ2016-75499-R (AEI/FEDER-UE)) for financial support and support through Severo Ochoa Excellence Accreditation 2014–2018 (SEV-2013-0319).

Supporting Information

The Supporting Information is available free of charge on the ACS Publications website at …. Reaction schemes for the formation of observed bi-products, catalytic tests with Zr and precious metal (Rh, Rh, Pd) promoted CeO_2, XRD patterns (before and after the reaction) and Raman spectra of CeO_2 and REM-CeO_2 materials, CO_2-/NH_3-TPD and H_2-TPR results, Raman and IR spectra of the catalysts after the reaction, TGA results of the catalysts before and after the reaction, BET surface area and pore volume of all studied materials.

AUTHOR INFORMATION

Corresponding author

aurakawa@iciq.es

Present address

§ The Swiss-Norwegian Beamlines (SNBL) at ESRF, CS40220, 38043 Grenoble CEDEX 9, France

References

1. Shaikh, A.-A. G.; Sivaram, S., Organic Carbonates. *Chem. Rev.* **1996,** *96*, 951–976.
2. Sakakura, T.; Choi, J.-C.; Yasuda, H., Transformation of Carbon Dioxide. *Chem. Rev.* **2007,** *107*, 2365–2387.
3. Sakakura, T.; Kohno, K., The Synthesis of Organic Carbonates from Carbon Dioxide. *Chem. Commun.* **2009**, 1312-1330.
4. Ono, Y., Catalysis in the Production and Reactions of Dimethyl Carbonate, an Environmentally Benign Building Block. *Appl. Catal. A-Gen.* **1997,** *155*, 133–166.
5. Aresta, M.; Quaranta, E., Carbon Dioxide: A Substitute for Phosgene. *ChemTech* **1997,** *27*, 32-40.
6. Keller, N.; Rebmann, G.; Keller, V., Catalysts, Mechanisms and Industrial Processes for the Dimethyl Carbonate Synthesis. *J. Mol. Catal. A-Chem.* **2010,** *317*, 1-18.
7. Delledonne, D.; Rivetti, F.; Romano, U., Developments in the Production and Application of Dimethyl Carbonate. *Appl. Catal. A-Gen.* **2001,** *221*, 241–251.
8. Pacheco, M. A.; Marshall, C. L., Review of Dimethyl Carbonate (DMC) Manufacture and Its Characteristics as a Fuel Additive. *Energ. Fuel.* **1997,** *11*, 2–29.
9. Tomishige, K.; Ikeda, Y.; Sakaihori, T.; Fujimoto, K., Catalytic Properties and Structure of Zirconia Catalysts for Direct Synthesis of Dimethyl Carbonate from Methanol and Carbon Dioxide. *J. Catal.* **2000,** *192*, 355–362.
10. Tomishige, K.; Sakaihori, T.; Ikeda, Y.; Fujimoto, K., A Novel Method of Direct Synthesis of Dimethyl Carbonate from Methanol and Carbon Dioxide Catalyzed by Zirconia. *Catal. Lett.* **1999,** *58*, 225-229.
11. Tomishige, K., Direct Synthesis of Dimethyl Carbonate from Methanol and Carbon Dioxide over Solid Oxide Catalysts. *Curr. Top. Catal.* **2002,** *3*, 81 - 101.
12. Wu, X. L.; Xiao, M.; Meng, Y. Z.; Lu, Y. X., Direct Synthesis of Dimethyl Carbonate on H_3PO_4 Modified V_2O_5. *J. Mol. Catal. A-Chem.* **2005,** *238*, 158–162.
13. Wu, X. L.; Meng, Y. Z.; Xiao, M.; Lu, Y. X., Direct Synthesis of Dimethyl Carbonate (DMC) Using Cu-Ni/VSO as Catalyst. *J. Mol. Catal. A-Chem.* **2006,** *249*, 93–97.
14. Ikeda, Y.; Sakaihori, T.; Tomishige, K.; Fujimoto, K., Promoting Effect of Phosphoric Acid on Zirconia Catalysts in Selective Synthesis of Dimethyl Carbonate from Methanol and Carbon Dioxide. *Catal. Lett.* **2000,** *66*, 59-62.
15. Ikeda, Y.; Asadullah, M.; Fujimoto, K.; Tomishige, K., Structure of the Active Sites on H_3PO_4/ZrO_2 Catalysts for Dimethyl Carbonate Synthesis from Methanol and Carbon Dioxide. *J. Phys. Chem. B* **2001,** *105*, 10653–10658.
16. Tomishige, K.; Furusawa, Y.; Ikeda, Y.; Asadullah, M.; Fujimoto, K., CeO_2–ZrO_2 Solid Solution Catalyst for Selective Synthesis of Dimethyl Carbonate from Methanol and Carbon Dioxide. *Catal. Lett.* **2001,** *76*, 71-74.
17. Tomishige, K.; Kunimori, K., Catalytic and Direct Synthesis of Dimethyl Carbonate Starting from Carbon Dioxide Using CeO_2-ZrO_2 Solid Solution Heterogeneous Catalyst: Effect of H_2O Removal from the Reaction System. *Appl. Catal. A-Gen.* **2002,** *237*, 103–109.
18. Hofmann, H. J.; Brandner, A.; Claus, P., Direct Synthesis of Dimethyl Carbonate by Carboxylation of Methanol on Ceria-Based Mixed Oxides. *Chem. Eng. Technol.* **2012,** *35*, 2140–2146.
19. Yoshida, Y.; Arai, Y.; Kado, S.; Kunimori, K.; Tomishige, K., Direct Synthesis of Organic Carbonates from the Reaction of CO_2 with Methanol and Ethanol over CeO_2 Catalysts. *Catal. Today* **2006,** *115*, 95–101.
20. Aresta, M.; Dibenedetto, A.; Pastore, C.; Cuocci, C.; Aresta, B.; Cometa, S.; Giglio, E. D., Cerium (IV) Oxide Modification by Inclusion of a Hetero-Atom: A Strategy for Producing Efficient and Robust Nano-Catalysts for Methanol Carboxylation. *Catal. Today* **2008,** *137*, 125–131.

21. Aresta, M.; Dibenedetto, A.; Pastore, C.; Angelini, A.; Aresta, B.; Pápai, I., Influence of Al2O3 on the Performance of CeO_2 Used as Catalyst in the Direct Carboxylation of Methanol to Dimethyl Carbonate and the Elucidation of the Reaction Mechanism. *J. Catal.* **2010,** *269*, 44–52.
22. Santos, B. A. V.; Silva, V. M. T. M.; Loureiro, J. M.; Barbosa, D.; Rodrigues, A. E., Modeling of Physical and Chemical Equilibrium for the Direct Synthesis of Dimethyl Carbonate at High Pressure Conditions. *Fluid Phase Equilibr.* **2012,** *336*, 41–51.
23. Santos, B. A. V.; Pereira, C. S. M.; Silva, V. M. T. M.; Loureiro, J. M.; Rodrigues, A. E., Kinetic Study for the Direct Synthesis of Dimethyl Carbonate from Methanol and CO_2 over CeO_2 at High Pressure Conditions. *Appl. Catal. A-Gen.* **2013,** *455*, 219–226.
24. Bansode, A.; Urakawa, A., Continuous DMC Synthesis from CO_2 and Methanol over a CeO_2 Catalyst in a Fixed Bed Reactor in the Presence of a Dehydrating Agent. *ACS Catal.* **2014,** *4*, 3877–3880.
25. Santos, B. A. V.; Silva, V. M. T. M.; Loureiro, J. M.; Rodrigues, A. E., Adsorption of H_2O and Dimethyl Carbonate at High Pressure over Zeolite 3A in Fixed Bed Column. *Ind. Eng. Chem. Res.* **2014,** *53*, 2473–2483.
26. Li, C.-F.; Zhong, S.-H., Study on Application of Membrane Reactor in Direct Synthesis DMC from CO_2 and CH_3OH over Cu–KF/MgSiO Catalyst. *Catal. Today* **2003,** *82*, 83–90.
27. Honda, M.; Tamura, M.; Nakagawa, Y.; Sonehara, S.; Suzuki, K.; Fujimoto, K.-i.; Tomishige, K., Ceria-Catalyzed Conversion of Carbon Dioxide into Dimethyl Carbonate with 2-Cyanopyridine. *ChemSusChem* **2013,** *6*, 1341–1344.
28. Honda, M.; Tamura, M.; Nakagawa, Y.; Nakao, K.; Suzuki, K.; Tomishige, K., Organic Carbonate Synthesis from CO_2 and Alcohol over CeO_2 with 2-Cyanopyridine: Scope and Mechanistic Studies. *J. Catal.* **2014,** *318*, 95–107.
29. Stoian, D.; Bansode, A.; Medina, F.; Urakawa, A., Catalysis under Microscope: Unraveling the Mechanism of Catalyst De- and Re-Activation in the Continuous Dimethyl Carbonate Synthesis from CO_2 and Methanol in the Presence of a Dehydrating Agent. *Catal. Today* **2017,** *283*, 2-10.
30. Eta, V.; Maki-Arvela, P.; Leino, A.-R.; Kordas, K.; Salmi, T.; Murzin, D. Y.; Mikkola, J.-P., Synthesis of Dimethyl Carbonate from Methanol and Carbon Dioxide: Circumventing Thermodynamic Limitations. *Ind. Eng. Chem. Res.* **2010,** *49*, 9609–9617.
31. Zhang, Z.-F.; Liu, Z.-W.; Lu, J.; Liu, Z.-T., Synthesis of Dimethyl Carbonate from Carbon Dioxide and Methanol over $Ce_xZr_{1-x}O_2$ and [EMIM]Br/$Ce_{0.5}Zr_{0.5}O_2$. *Ind. Eng. Chem. Res.* **2011,** *50*, 1981–1988.
32. Trovarelli, A., *Catalysis by Ceria and Related Materials*. Imperial College Press: 2002.
33. Trovarelli, A., Catalytic Properties of Ceria and CeO_2-Containing Materials. *Catal. Rev.* **1996,** *38*, 439-520.
34. Trovarelli, A., Structural and Oxygen Storage/Release Properties of CeO_2-Based Solid Solutions. *Comment. Inorg. Chem.* **1999,** *20*, 263-284.
35. Gorte, R. J., Ceria in Catalysis: From Automotive Applications to the Water–Gas Shift Reaction. *AIChE J.* **2010,** *56*, 1126–1135.
36. Steele, B. C. H.; Heinzel, A., Materials for Fuel-Cell Technologies. *Nature* **2001,** *414*, 345-352.
37. Reddy, B. M.; Katta, L.; Thrimurthulu, G., Novel Nanocrystalline $Ce_{1-x}La_xO_{2-\delta}$ (x = 0.2) Solid Solutions: Structural Characteristics and Catalytic Performance. *Chem. Mater.* **2010,** *22*, 467–475.
38. Moura, J. S.; Fonseca, J. d. S. L.; Bion, N.; Epron, F.; Silva, T. d. F.; Maciel, C. G.; Assaf, J. M.; Rangel, M. d. C., Effect of Lanthanum on the Properties of Copper, Cerium and Zirconium Catalysts for Preferential Oxidation of Carbon Monoxide. *Catal. Today* **2014,** *228*, 40–50.
39. Miki, T.; Ogawa, T.; Haneda, M.; Kakuta, N.; Ueno, A.; Tateishi, S.; Matsuura, S.; Sato, M., Enhanced Oxygen Storage Capacity of Cerium Oxides in Cerium Dioxide/Lanthanum Sesquioxide/Alumina Containing Precious Metals. *J. Phys. Chem.* **1990,** *94*, 6464–6467.

40. Cho, B. K., Chemical Modification of Catalyst Support for Enhancement of Transient Catalytic Activity: Nitric Oxide Reduction by Carbon Monoxide over Rhodium. *J. Catal.* **1991,** *131*, 74-87.
41. Lee, J. G.; Park, J. H.; Shul, Y. G., Tailoring Gadolinium-Doped Ceria-Based Solid Oxide Fuel Cells to Achieve 2 W cm^{-2} at 550 °C. *Nat. Commun.* **2014,** *5:4045*.
42. Martínez-Arias, A.; Hungría, A. B.; Fernández-García, M.; Iglesias-Juez, A.; Soria, J.; Conesa, J. C.; Anderson, J. A.; Munuera, G., Operando DRIFTS Study of the Redox and Catalytic Properties of $CuO/Ce_{1-x}Tb_xO_{2-\delta}$ (x = 0–0.5) Catalysts: Evidence of an Induction Step During CO Oxidation. *Phys. Chem. Chem. Phys.* **2012,** *14*, 2144-2151.
43. Reddy, B. M.; Thrimurthulu, G.; Katta, L., Design of Efficient $Ce_xM_{1-x}O_{2-\delta}$ (M = Zr, Hf, Tb and Pr) Nanosized Model Solid Solutions for CO Oxidation. *Catal. Lett.* **2011,** *141*, 572-581.
44. Tang, Y.; Zhang, H.; Cui, L.; Ouyang, C.; Shi, S.; Tang, W.; Li, H.; Lee, J.-S.; Chen, L., First-Principles Investigation on Redox Properties of M-Doped CeO_2 (M = Mn, Pr, Sn, Zr). *Phys. Rev. B* **2010,** *82*, 125104
45. Ahn, K.; Yoo, D. S.; Prasad, D. H.; Lee, H.-W.; Chung, Y.-C.; Lee, J.-H., Role of Multivalent Pr in the Formation and Migration of Oxygen Vacancy in Pr-Doped Ceria: Experimental and First-Principles Investigations. *Chem. Mater.* **2012,** *24*, 4261–4267.
46. Tamura, M.; Wakasugi, H.; Shimizu, K.-i.; Satsuma, A., Efficient and Substrate-Specific Hydration of Nitriles to Amides in Water by Using a CeO_2 Catalyst. *Chem. Eur. J.* **2011,** *17*, 11428–11431.
47. Zarembowitch, J.; Gouteron, J.; Lejus, A. M., Raman Spectra of Lanthanide Sesquioxide Single Crystals with A-Type Structure. *Phys. stat. sol. (b)* **1979,** *94*, 249-256.
48. Westermann, A.; Geantet, C.; Vernoux, P.; Loridant, S., Defects Band Enhanced by Resonance Raman Effect in Praseodymium Doped CeO_2. *J. Raman Spectrosc.* **2016,** *47*, 1276–1279.
49. Guo, M.; Lu, J.; Wu, Y.; Wang, Y.; Luo, M., UV and Visible Raman Studies of Oxygen Vacancies in Rare-Earth-Doped Ceria. *Langmuir* **2011,** *27*, 3872-3877.
50. Cutrufello, M. G.; Ferino, I.; Solinas, V.; Primavera, A.; Trovarelli, A.; Auroux, A.; Picciau, C., Acid–Base Properties and Catalytic Activity of Nanophase Ceria–Zirconia Catalysts for 4-Methylpentan-2-ol Dehydration. *Phys. Chem. Chem. Phys.* **1999,** *1*, 3369-3375.
51. Wada, S.; Oka, K.; Watanabe, K.; Izumi, Y., Catalytic Conversion of Carbon Dioxide into Dimethyl Carbonate Using Reduced Copper-Cerium Oxide Catalysts as Low as 353 K and 1.3 MPa and the Reaction Mechanism. *Front. Chem.* **2013,** *1*, 1-8.
52. Hahn, K. R.; Iannuzzi, M.; Seitsonen, A. P.; Hutter, J., Coverage Effect of the CO_2 Adsorption Mechanisms on CeO_2(111) by First Principles Analysis. *J. Phys. Chem. C* **2013,** *117*, 1701–1711.
53. Choudhary, V. R.; Rane, V. H., Acidity/Basicity of Rare-Earth Oxides and their Catalytic Activity in Oxidative Coupling of Methane to C2-Hydrocarbons. *J. Catal.* **1991,** *130*, 411-422.
54. Ikeda, Y.; Furusawa, Y.; Tomishige, K.; Fujimoto, K., Selective Conversion of Carbon Dioxide and Methanol to Dimethyl Carbonate Using Phosphoric Acid-Modified Zirconia Catalysts. *ACS Symp. Ser.* **2002,** *809*, 71–84.
55. Jung, K. T.; Bell, A. T., An in Situ Infrared Study of Dimethyl Carbonate Synthesis from Carbon Dioxide and Methanol over Zirconia. *J. Catal.* **2001,** *204*, 339–347.
56. Migani, A.; Vayssilov, G. N.; Bromley, S. T.; Illas, F.; Neyman, K. M., Dramatic Reduction of the Oxygen Vacancy Formation Energy in Ceria Particles: A Possible Key to their Remarkable Reactivity at the Nanoscale. *J. Mater. Chem.* **2010,** *20*, 10535-10546.
57. Sutradhar, N.; Sinhamahapatra, A.; Pahari, S.; Jayachandran, M.; Subramanian, B.; Bajaj, H. C.; Panda, A. B., Facile Low-Temperature Synthesis of Ceria and Samarium-Doped Ceria Nanoparticles and Catalytic Allylic Oxidation of Cyclohexene. *J. Phys. Chem. C* **2011,** *115*, 7628–7637.

58. Meher, S. K.; Rao, G. R., Polymer-Assisted Hydrothermal Synthesis of Highly Reducible Shuttle-Shaped CeO_2: Microstructural Effect on Promoting Pt/C for Methanol Electrooxidation. *ACS Catal.* **2012,** *2*, 2795–2809.
59. Yao, H. C.; Yao, Y. F. Y., Ceria in Automotive Exhaust Catalysts: I. Oxygen Storage. *J. Catal.* **1984,** *86*, 254-265.
60. Giordano, F.; Trovarelli, A.; Leitenburg, C. d.; Giona, M., A Model for the Temperature-Programmed Reduction of Low and High Surface Area Ceria. *J. Catal.* **2000,** *193*, 273–282.
61. Prymak, I.; Kalevaru, V. N.; Wohlrab, S.; Martin, A., Continuous Synthesis of Diethyl Carbonate from Ethanol and CO_2 over Ce–Zr–O Catalysts *Catal. Sci. Technol.* **2015,** *5*, 2322-2331.
62. Pojanavaraphan, C.; Luengnaruemitchai, A.; Gulari, E., Effect of Catalyst Preparation on $Au/Ce_{1-x}Zr_xO_2$ and $Au–Cu/Ce_{1-x}Zr_xO_2$ for Steam Reforming of Methanol. *Int. J. Hydrogen Energ.* **2013,** *38*, 1348–1362.
63. Dobrosz-Gómez; Gómez-García, M. Á.; Rynkowski, J. M., CO Oxidation over Au/CeO_2-ZrO_2 Catalists: The Effect of the Support Composition of the Au-Support Interaction. *Kinet. Catal.* **2010,** *51*, 823–827.
64. Jin, Q.; Shen, Y.; Zhu, S., Praseodymium Oxide Modified CeO_2/Al_2O_3 Catalyst for Selective Catalytic Reduction of NO by NH_3. *Chin. J. Chem.* **2016,** *34*, 1283—1290.
65. Tamura, M.; Kishi, R.; Nakayama, A.; Nakagawa, Y.; Hasegawa, J.-y.; Tomishige, K., Formation of a New, Strongly Basic Nitrogen Anion by Metal Oxide Modification. *J. Am. Chem. Soc.* **2017,** *139*, 11857−11867.
66. Badri, A.; Binet, C.; Lavalley, J.-C., Use of Methanol as an IR Molecular Probe to Study the Surface of Polycrystalline Ceria. *J. Chem. Soc., Faraday Trans.* **1997,** *93*, 1159-1168.
67. Tamura, M.; Satsuma, A.; Shimizu, K.-i., CeO_2-Catalyzed Nitrile Hydration to Amide: Reaction Mechanism and Active Sites. *Catal. Sci. Technol.* **2013,** *3*, 1386-1393.
68. Tamura, M.; Tomishige, K., Redox Properties of CeO_2 at Low Temperature: The Direct Synthesis of Imines from Alcohol and Amine. *Angew. Chem. Int. Ed.* **2015,** *54*, 864 –867.
69. D'Angelo, A. M.; Wu, Z.; Overbury, S. H.; Chaffee, A. L., Cu-Enhanced Surface Defects and Lattice Mobility of Pr-CeO_2 Mixed Oxides. *J. Phys. Chem. C* **2016,** *120*, 27996–28008.

Supporting Information

Improving the stability of CeO_2 catalyst by rare earth metal promotion and molecular insights in the dimethyl carbonate synthesis from CO_2 and methanol with 2-cyanopyridine

Dragos Stoian[†, ‡, §], Francisco Medina[‡], Atsushi Urakawa[*†]

[†] Institute of Chemical Research of Catalonia (ICIQ), The Barcelona Institute of Science and Technology, Av. Països Catalans 16, 43007 Tarragona, Spain

[‡] Department of Chemical Engineering, University Rovira i Virgili, Av. Països Catalans 26, 43007 Tarragona, Spain

*Email: aurakawa@iciq.es

Present address

[§] The Swiss-Norwegian Beamlines (SNBL) at ESRF, CS40220, 38043 Grenoble CEDEX 9, France

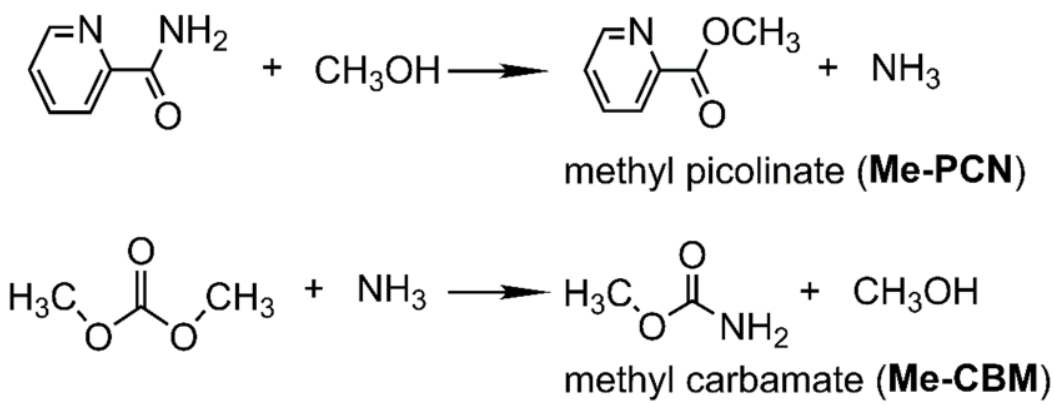

Scheme S1. By-products formation (methyl picolinate, Me-PCN and methyl carbamate, Me-CBM) in the continuous DMC synthesis in the presence of a dehydrating agent (2-cyanopyridine, 2-CP). 2-CP hydrolysis leads to the formation of the corresponding amide, 2-picolinamide, 2-PA.

Experimental: materials

High surface area powders of CeO_2 and CeO_2-ZrO_2 solid solutions (78-22, 50-50, and 25-75 wt%) were kindly supplied by Daiichi Kigenso Kagaku Kogyo Co. Ltd., Japan and used without any further treatment. High surface area ZrO_2 (1/8" pellets) was purchased from Alfa Aesar and used as received. Precious metals (1 wt% Ru, Rh, Pd) were synthesized by the incipient wetness impregnation of the pristine CeO_2 with an aqueous solution of the metal precursor (chlorides). The metal chlorides (99.9% purity) were purchased from Alfa Aesar. The impregnated materials were dried overnight at 80-90 °C in an oven and calcined at 400 °C for 4 h in a static air after a temperature ramp of 2 °C min^{-1}.

Direct methanol carboxylation: effect of Zr and precious metal (PM)

Figure S1 (a) shows the catalytic performance in terms of methanol conversion (X_{MeOH}) and DMC selectivity (S_{DMC}) during the initial phase (0-2 h) and at 24-26 h of the DMC synthesis using CeO_2, ZrO_2 and CeO_2-ZrO_2 solid solutions. The reaction time, more precisely time on stream, is shown as 2 h interval due to the residence time of the liquid solution in the reaction system. The liquid sample was analyzed every 2 h when enough liquid product (ca. 1 mL) was collected (when one number is shown for the reaction time, the initial value of the interval is taken). Although the addition of Zr to CeO_2 has been reported to positively affect the catalytic activity[1-5] for the reaction, in this work negative effects of Zr incorporation were obvious. Regarding the initial activity (0-2 h), the decrease in X_{MeOH} became consistently more prominent at higher Zr content, decreasing from 92.4%, 88.4%, 72.9% to 37.3% for 0, 22, 50, and 75 wt% ZrO_2 amount in the solid solution, respectively. Moreover, the use of high surface area ZrO_2 gave only a trace amount of DMC. After 24 h, catalyst deactivation was observed for all catalysts and it was more pronounced for Ce-Zr [50/50] (ca. 21% activity drop compared to 6-8% drops of the other samples). On the other hand, the drop in catalytic activity did not affect S_{DMC} significantly, showing >95% with the formation of small amounts of Me-PCN (from 1.0 to 4.3%) and Me-CBM (0.4 to 1.6%). Interestingly, at higher ZrO_2 content in the solid solutions, the decrease in S_{DMC} was smaller over 24 h (ca. 5% S_{DMC} decrease for Ce-Zr [100/0], while only ca. 1% decrease for Ce-Zr [25/75]), indicating positive influences of Zr promotion on the catalyst stability in terms of DMC selectivity.

Figure S1 (b) presents the catalytic performance using CeO_2-supported Ru, Rh and Pd catalysts. Clearly, these results indicate strongly negative influences of the PMs on the

performance. For 1 wt% Pd-CeO_2 and 1 wt% Rh-CeO_2, ca. 63% X_{MeOH} was initially observed, while the addition of 1 wt% Ru resulted in much lower activity of 34% X_{MeOH}. Regarding the catalyst stability, it is very striking to note that both 1 wt% Rh-CeO_2 and 1 wt% Ru-CeO_2 catalysts showed a tremendous loss in activity after 24 h (X_{MeOH} of ca. 7 and 12%, respectively). In contrast, a slight increase in X_{MeOH} (from 63 to 70%) was detected for 1 wt% Pd-CeO_2. The incorporation of the PMs consistently impacted negatively on DMC selectivity, showing ca. 75-80% S_{DMC} for the three catalysts. Interestingly, unlike CeO_2 and CeO_2-ZrO_2 solid solutions, all ceria-supported PM catalysts displayed an increase in S_{DMC} by ca. 10% after 24 h of the reaction. Still, S_{DMC} values were considerably lower compared to that observed for CeO_2 and the by-products were 1.6-20.4% Me-PCN and 1.1-5.4% Me-CBM. The high selectivity to Me-PCN indicates that 2-PA is formed via the hydration reaction of 2-CP and that the reaction between 2-PA and methanol (**Scheme S1**) is promoted by the PMs or by the sites created by the specific interactions between CeO_2 with the PMs. The reaction is similar to urea methanolysis where -NH_2 group is replaced by -OCH_3 group and both acidic and basic catalysts are known to catalyze the reaction.[6-7] CeO_2-based materials are known to be active in the reaction[8-9], and it is implied that promotion of CeO_2 by the PMs can be highly effective for methanolysis reactions.

Generally, both Zr and PMs incorporation showed negative influences on the catalytic performance, especially on the reactivity (X_{MeOH}). The lower reactivity of the catalysts at higher Zr contents implies that the reactivity originates from CeO_2 and its surface. In case of PMs addition, the impact on the reactivity was drastic despite the relatively low amount of the PMs (1 wt%) with respect to CeO_2. Considering the much lower initial reactivity and

the very low catalytic stability of Rh-CeO_2 and Ru-CeO_2 compared to CeO_2, it can be concluded that the PMs alter the chemical surface properties (e.g. acid-base, redox) completely, as confirmed later. Nonetheless, the effects of incorporating both Zr and PMs in CeO_2 were found negative for the activity and stability in the reaction.

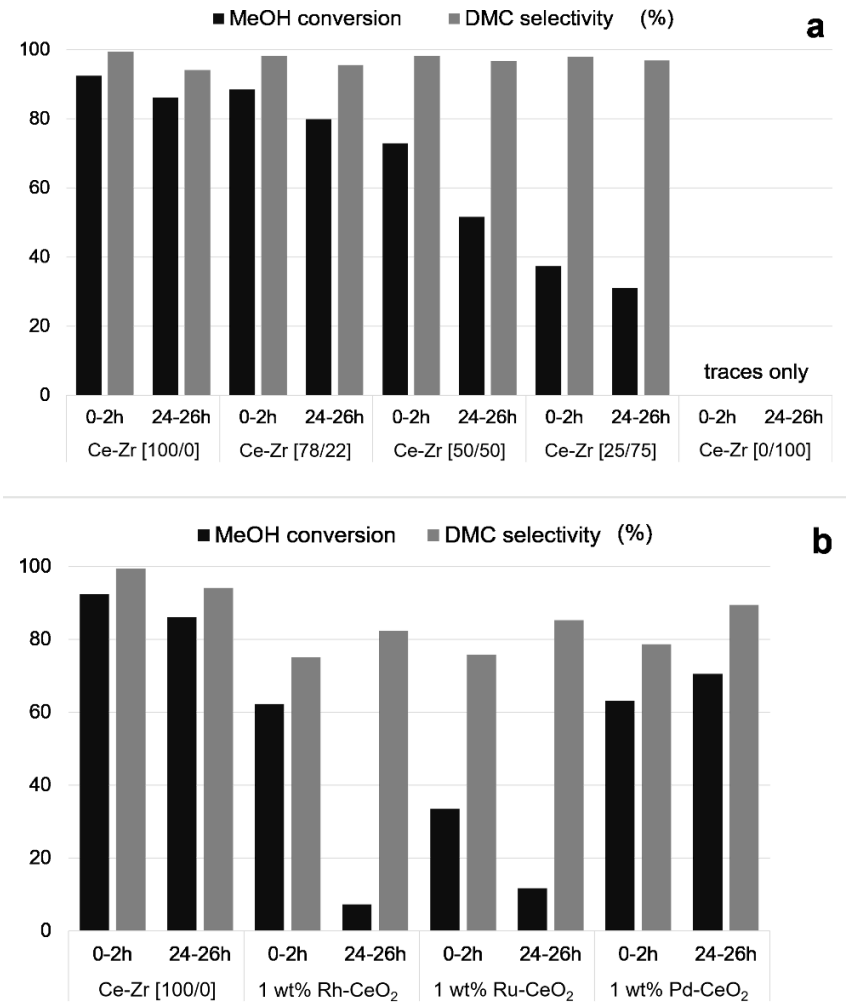

Figure S1. Methanol conversion and DMC selectivity during the continuous DMC synthesis at 120 °C, 30 bar at time on stream of 0-2 and 24-26 h using **a.** Ce-Zr mixed oxides and **b.** precious metal-CeO_2 as catalyst. Black and grey columns represent methanol conversion and DMC selectivity, respectively.

Characterization: structural and textural properties (XRD, Raman, N_2 physisorption)

The XRD patterns of the pristine CeO_2, CeO_2-ZrO_2 solid solutions, ZrO_2 and as-synthesized materials incorporating PM and REM are presented in **Figure S2**. CeO_2 showed the peaks corresponding to (111), (200), (220), and (311) planes of cubic fluorite phase, while ZrO_2 exhibited the peaks for a monoclinic phase with a small amount of a tetragonal phase. CeO_2-ZrO_2 solid solutions preserved a single cubic fluorite phase characteristic of CeO_2 without a detectable monoclinic/tetragonal phase characteristic of ZrO_2. It should be noted that the characteristic XRD peaks of CeO_2-ZrO_2 solid solutions slightly shifted to higher angles compared to the peaks for cubic fluorite phase of CeO_2. This can be explained by the insertion of zirconium atoms in the CeO_2 cubic matrix with the shrinkage of its unit cell (Ce^{4+} ionic radius is 0.97 Å, whereas Zr^{4+} ionic radius is 0.82 Å) and by the deformation of the cubic phase to be transformed into the tetragonal phase for higher zirconium loading.[10] The materials with PM and REM showed negligible structural changes, indicating that metal promoters were finely dispersed on the surface of the support.

Figure S3 shows the Raman spectra of 1wt% (left) and 5 wt% (right) REM-doped CeO_2 materials in comparison to the spectrum of pristine CeO_2. The major changes were observed for Pr-doped CeO_2 materials. The origin of the spectral changes and influence on catalytic activity are discussed in the main text.

The BET surface area and pore volume of all materials are presented in **Table S1**. Higher amount of incorporated Zr or REM to CeO_2 consistently decreased the surface area, although there was no clear trend in the pore volume with the type and loading of REM. In case of the PM-loaded materials, the surface area was also reduced and it was most

pronounced for Pd-CeO_2. The pore volume of the three PM-CeO_2 samples were similarly reduced by ca. 10%. Importantly, the changes in the textural properties and bulk structure of the materials are not correlated with the catalytic activity and stability.

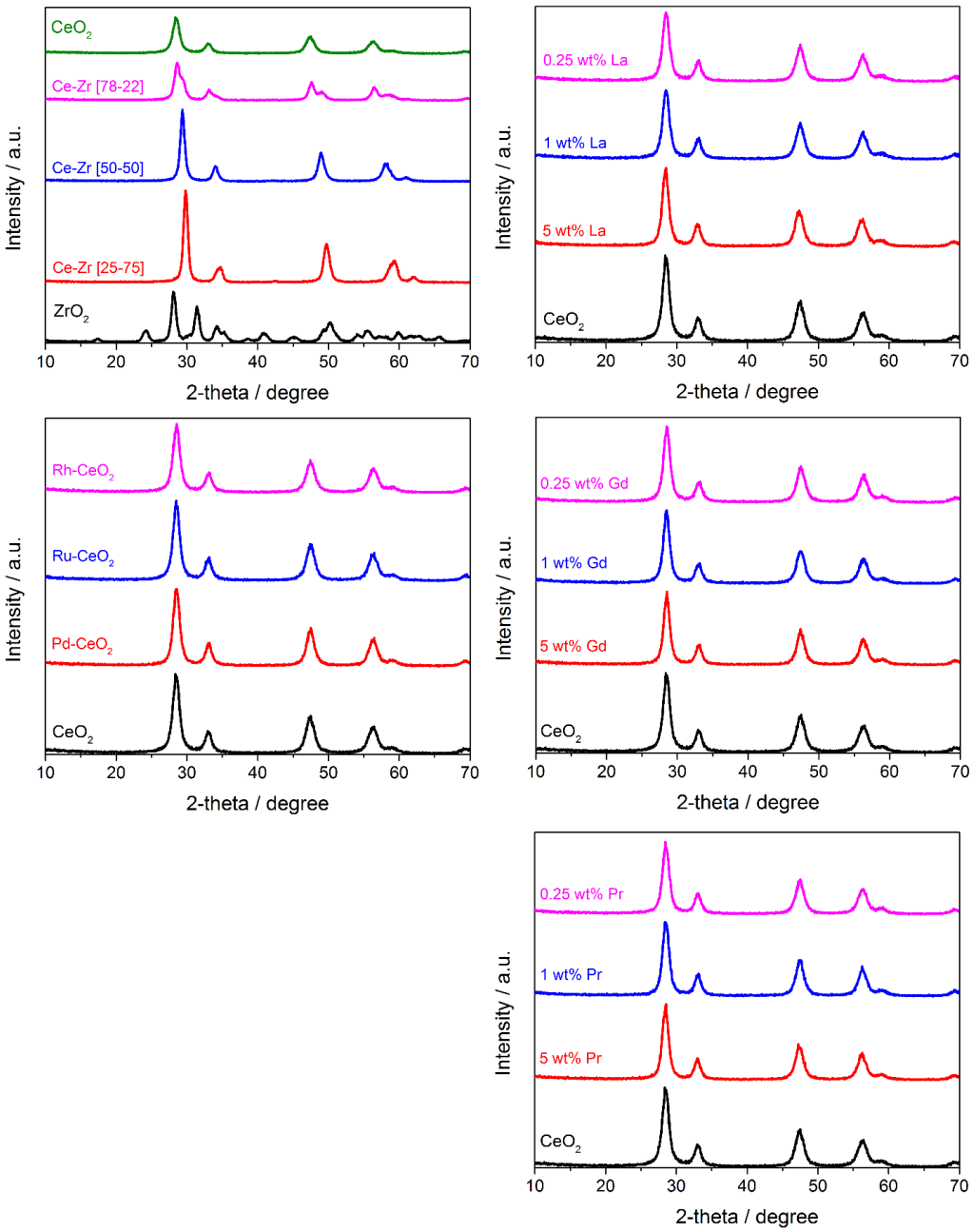

Figure S2. X-ray diffraction (XRD) patterns of the pristine CeO_2, CeO_2-ZrO_2 solid solutions, ZrO_2 and as-synthesized materials incorporating precious metal and REM promoters.

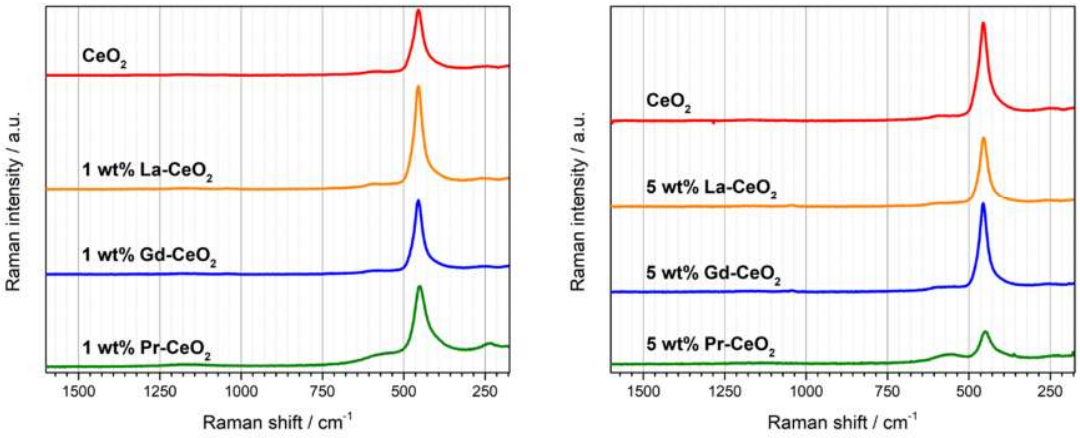

Figure S3. Raman spectra (excitation laser: 532 nm) of pristine CeO_2 (red) and REM (La (orange), Gd (blue) and Pr (green))-CeO_2. (left) 1 wt% REM-CeO_2 materials and (right) 5 wt% REM-CeO_2.

Characterization: acidity and basicity

Generally, the addition of a foreign atom on/in the CeO_2 structure reduced the amount of adsorbed CO_2/NH_3, thus the total number of acidic and basic sites. The exceptions were CeO_2-ZrO_2 solid solutions and ZrO_2 for which the weak acidity was greatly enhanced when the ZrO_2 content was >50 wt% due to more pronounced influence of highly acidic ZrO_2[11-14] in the solid solutions (**Figure S4 A**). Zr-addition to CeO_2 resulted in weakening of the strong acidity/basicity as indicated by the small amount of adsorbed NH_3/CO_2, respectively, at temperature above ca. 500 °C.

On the other hand, PM addition to CeO_2 induced remarkable changes in the acidity/basicity of the material (**Figure S4 A**). Upon Rh and Ru addition to CeO_2, weak and moderate acidic sites were decreased, but mildly strong acidic sites (desorption at ca. 520 °C) became less and, in contrast, highly strong acidity (desorption at ca. 700 °C) was enhanced. For Rh- and Ru-CeO_2, the number of strong basic sites were reduced

significantly, although the formation of stronger basic sites characterized by the desorption peaks at 680 and 760 °C was observed for Ru-CeO_2. Pd addition resulted in very different changes in both acidity and basicity from those of Rh and Ru addition. Notably, the weak-moderate basicity of CeO_2, characterized by the broad CO_2 desorption peaks in the range of 100-450 °C, was largely suppressed and, instead, strong basic sites (desorption at ca. 640 °C) were formed. The similarity of acid-base properties of Rh- and Ru-CeO_2 in comparison to Pd-CeO_2 was consistently reflected in the catalytic activity and stability trend (**Figure S1**). This implies that acid-base properties are playing roles in the DMC synthesis from CO_2 and methanol in the presence of 2-CP.

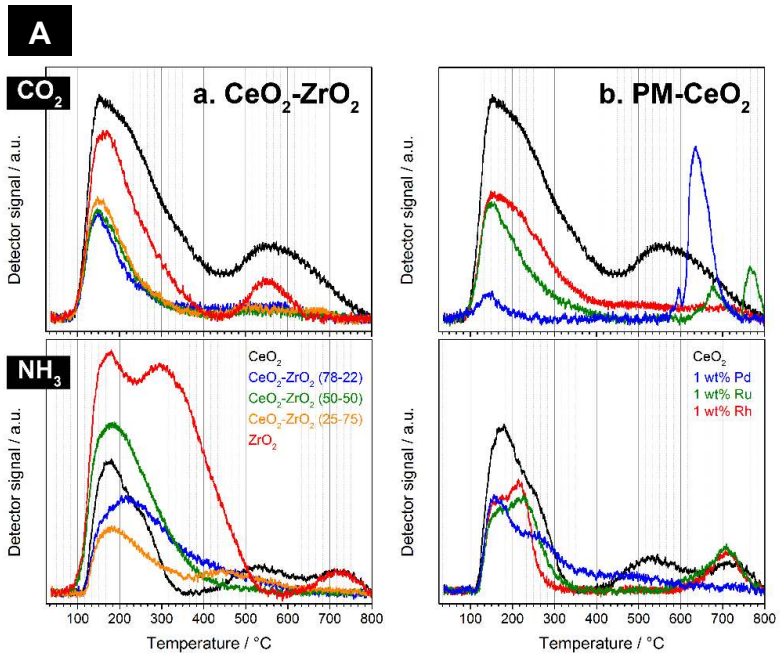

Figure S4 (A). Temperature programmed desorption (TPD) profiles of the CeO_2-ZrO_2 solid solutions and precious metals (PM) promoted CeO_2 materials. Upper panels correspond to those of CO_2-TPD, whereas the lower ones to those of NH_3-TPD.

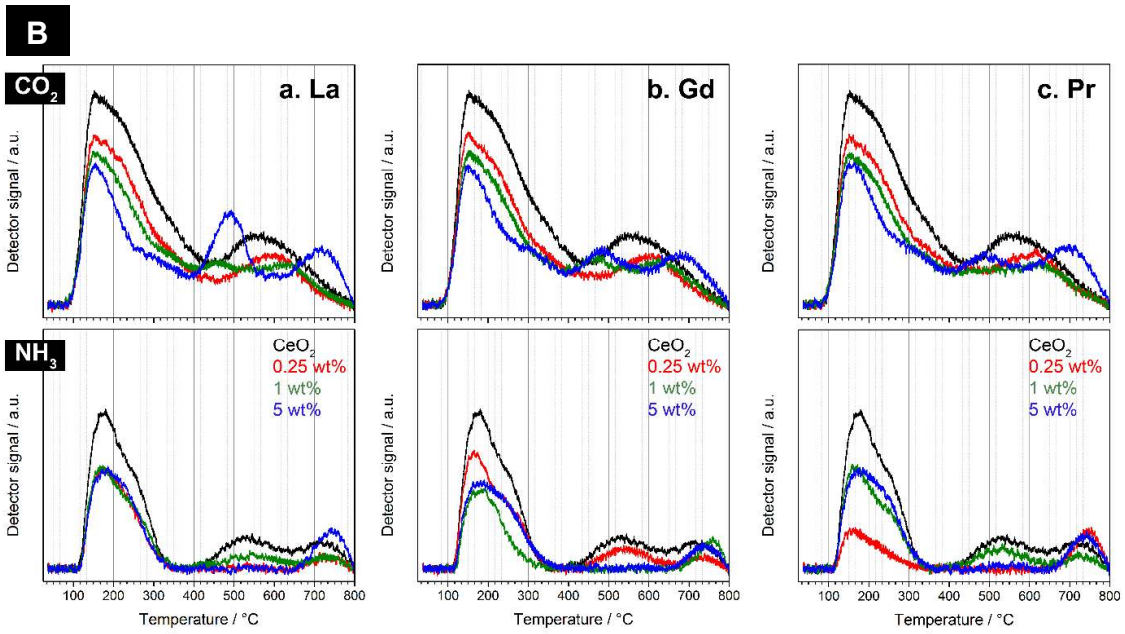

Figure S4 (B). Temperature programmed desorption (TPD) profiles of the rare earth metals (REM) promoted CeO_2 materials. Upper panels correspond to those of CO_2-TPD, whereas the lower ones to those of NH_3-TPD.

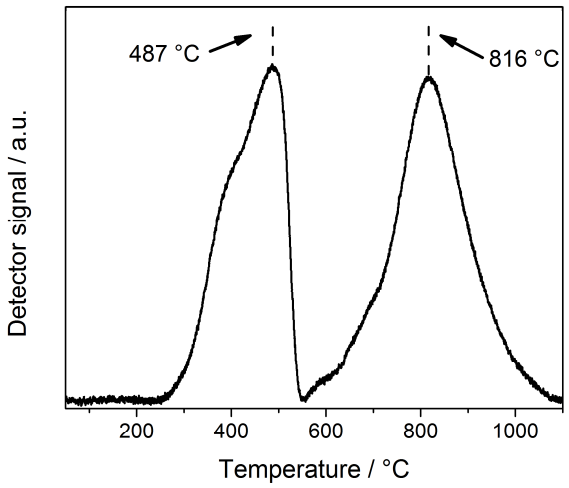

Figure S5. H_2-TPR profiles of the high surface area CeO_2 used throughout this study. Both surface (low temperature) and bulk (high temperature) reduction peaks can be clearly identified.

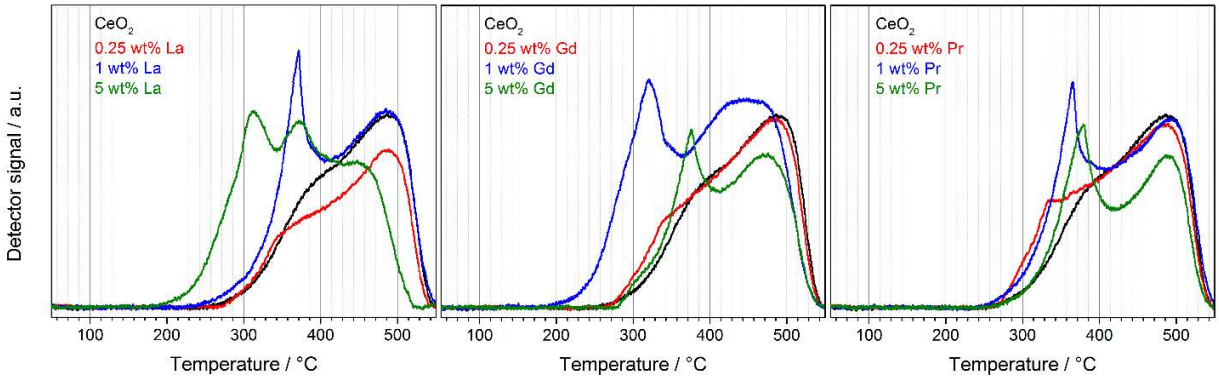

Figure S6. H_2-TPR profiles of the REM-CeO_2 materials used throughout this study. Surface reduction peak is represented.

As well known, Zr addition to CeO_2 induced drastic changes in the reducibility of CeO_2[15-17] (**Figure S7**). The TPR profiles of the CeO_2-ZrO_2 solid solutions displayed only one main broad reduction peak in the region between 500–580 °C at different peak positions (507, 543, and 576 °C for CeO_2-ZrO_2 [78-22], [50-50], and [25-75], respectively). In contrast, the high surface area ZrO_2 used in the present study showed no reduction peaks under the condition investigated (**Figure S7**). Although the overall reducibility of CeO_2-ZrO_2 is enhanced by facilitating the bulk reduction compared to CeO_2, it should be noted that the reduction of surface Ce atoms is more facile for CeO_2 than CeO_2-ZrO_2 at lower temperatures (<400 °C, **Figure S5**). The catalytic tests clearly showed that CeO_2 and not ZrO_2 is responsible for activation of CO_2 and methanol (**Figure S1**), and this indicates that the reducibility of surface Ce may play important role in the reaction mechanisms besides the balance between basic/acidic sites. The importance of redox sites in the catalytic cycle have been investigated by *operando* spectroscopic means and will be communicated separately.

PM addition to CeO_2 resulted in totally different TPR profiles (**Figure S8**). The three catalysts are characterized by the appearance of a new large peak in the TPR profiles at

very low temperatures around 100-180 °C, characteristic of Ru, Rh, and Pd oxides reduction. The peak corresponding to the CeO_2 surface reduction was reduced drastically for the three PM-CeO_2 materials. As in the cases of the catalytic activity (**Figure S1**) and TPD results (**Figure S4**), the reducibility of Ru- and Rh-CeO_2 presented some similarities, showing the reduction peak at ca. 100 °C, while a higher reduction peak ca. 180 °C was observed for Pd-CeO_2. This indicates possible correlations among catalyst reducibility, acidity-basicity, and catalytic performance. Based on the H_2-TPR profiles of PM-CeO_2, the H_2 consumption is high at low temperatures below 200 °C considering that it is the reduction of 1 wt% PM. This observation together with lowered reduction peak at ca. 500 °C imply the promoted reduction of surface Ce by the catalytic function of PM, facilitating the reactivity of surface oxygen of CeO_2. Nevertheless, this high reducibility of surface CeO_2 did not positively affect the catalytic performance of PM-CeO_2 (**Figure S1**) and further investigation is required to elucidate the PM effects on the reactivity and product selectivity.

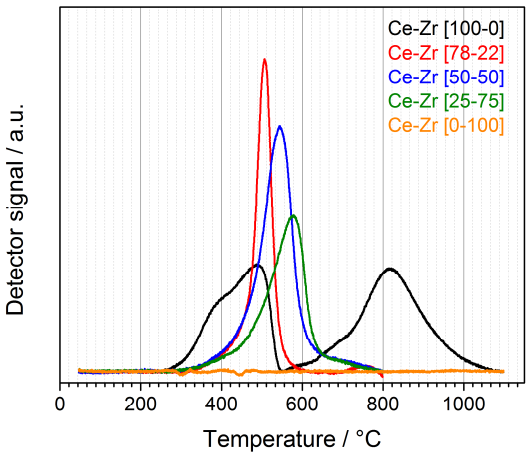

Figure S7. H_2-TPR profiles of the CeO_2-ZrO_2 solid solutions (black for pure CeO_2 and orange for pure ZrO_2).

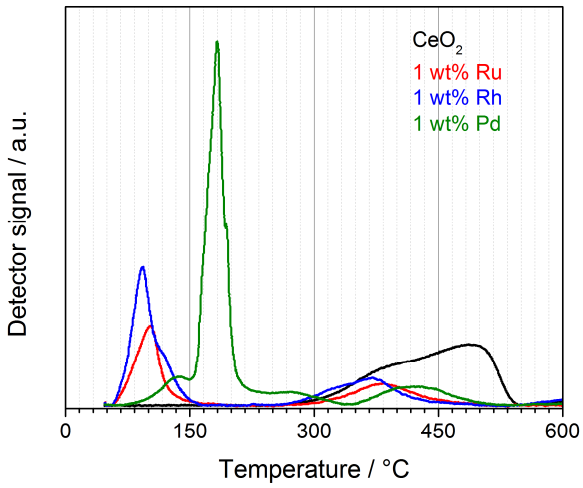

Figure S8. H_2-TPR profiles of the precious metals (PM) promoted CeO_2 materials (surface reduction region).

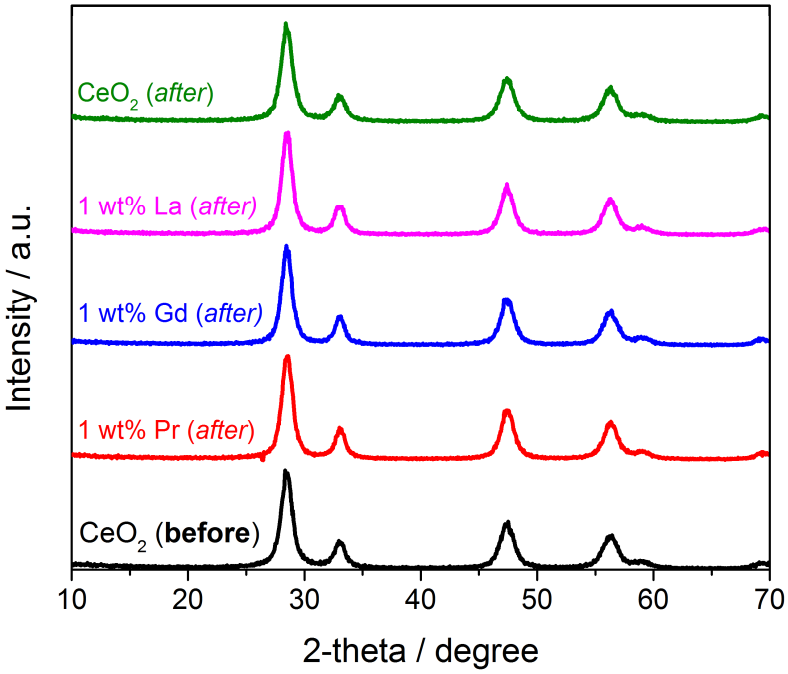

Figure S9. XRD patterns of the used materials (CeO_2 and 1 wt% REM promoted CeO_2) after the 30 h catalytic comparison test.

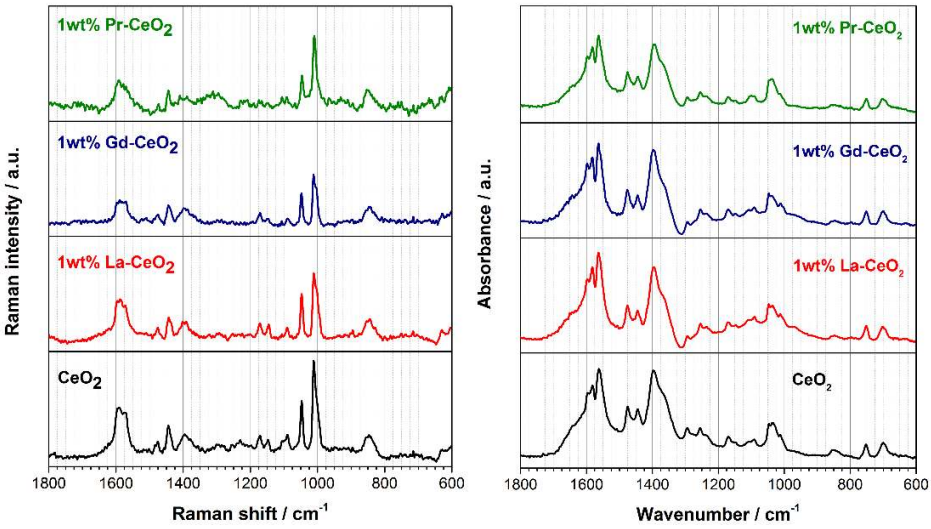

Figure S10. Raman (**left**) and ATR-IR (**right**) studies of the catalysts after the reaction and methanol washing. The spectral contribution due to CeO_2 has been subtracted and the Raman spectra have been normalized with respect to CeO_2 F_{2g} mode at ca. 460 cm^{-1}.

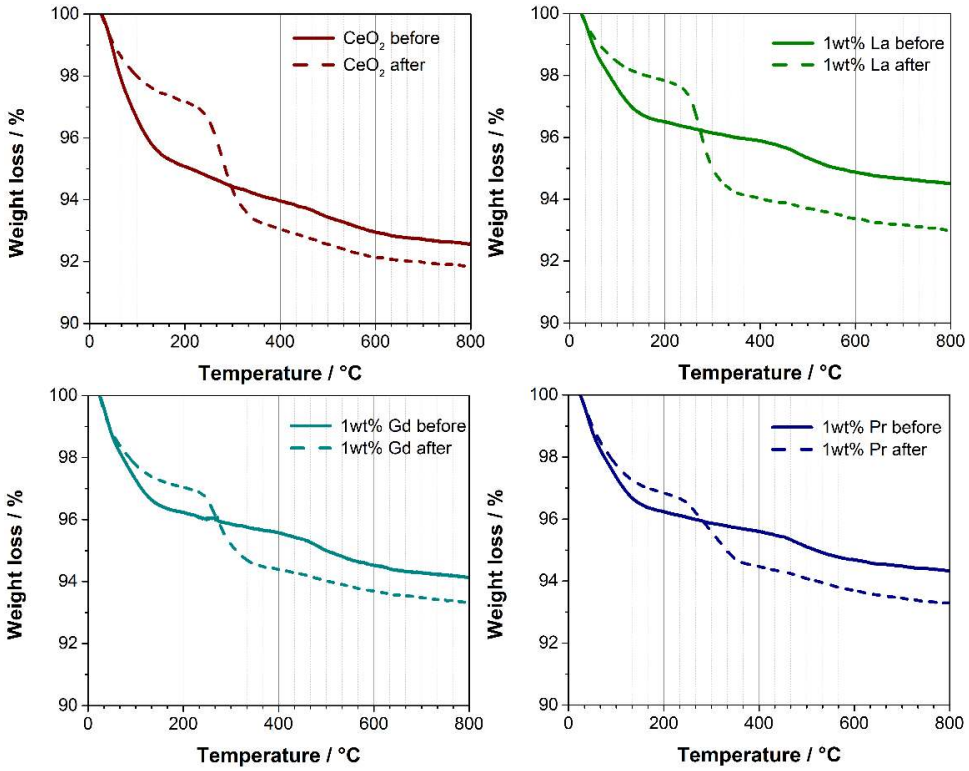

Figure S11. TGA of CeO_2 and 1 wt% REM promoted CeO_2 before and after the reaction.

Table S1. The BET surface area ($m^2\ g^{-1}$) and pore volume ($cm^3\ g^{-1}$) of the pristine CeO_2, CeO_2-ZrO_2 solid solutions, ZrO_2 and as-synthesized materials incorporating precious metal and rare earth metal promoters.

Material type		BET surface area ($m^2\ g^{-1}$)	Pore volume ($cm^3\ g^{-1}$)
CeO_2-ZrO_2 solid solutions	CeO_2	160	0.197
	CeO_2-ZrO_2 [78-22]	75	0.247
	CeO_2-ZrO_2 [50-50]	59	0.199
	CeO_2-ZrO_2 [25-75]	58	0.230
	ZrO_2	97	0.320
Precious metals (PM) – CeO_2	1 wt% Rh-CeO_2	141	0.173
	1 wt% Ru-CeO_2	147	0.176
	1 wt% Pd-CeO_2	123	0.177
Rare earth metals (REM) – CeO_2	0.25 wt% La-CeO_2	149	0.175
	1 wt% La-CeO_2	135	0.186
	5 wt% La-CeO_2	122	0.172
	0.25 wt% Gd-CeO_2	156	0.198
	1 wt% Gd-CeO_2	146	0.199
	5 wt% Gd-CeO_2	123	0.177
	0.25 wt% Pr-CeO_2	152	0.180
	1 wt% Pr-CeO_2	139	0.184
	5 wt% Pr-CeO_2	126	0.173

Table S2. The amounts of adsorbed-desorbed CO_2 and NH_3 expressed in µmol $g_{cat.}^{-1}$ (a measure of the basicity and acidity of the materials) for the catalysts tested in the long term studies of DMC synthesis.

Material type		µmol CO_2 $g_{cat.}^{-1}$	µmol NH_3 $g_{cat.}^{-1}$
CeO_2-ZrO_2 solid solutions	CeO_2	520.8	396.2
	CeO_2-ZrO_2 [78-22]	140.1	511.2
	CeO_2-ZrO_2 [50-50]	137.7	710.0
	CeO_2-ZrO_2 [25-75]	149.0	316.3
	ZrO_2	313.6	1410.8
Precious metal (PM) – CeO_2	1 wt% Rh-CeO_2	259.6	255.8
	1 wt% Ru-CeO_2	176.8	299.5
	1 wt% Pd-CeO_2	118.1	360.1
Rare earth metal (REM) – CeO_2	0.25 wt% La-CeO_2	411.7	259.3
	1 wt% La-CeO_2	380.3	317.9
	5 wt% La-CeO_2	399.0	308.7
	0.25 wt% Gd-CeO_2	410.8	364.3
	1 wt% Gd-CeO_2	377.1	243.0
	5 wt% Gd-CeO_2	386.2	286.1
	0.25 wt% Pr-CeO_2	414.5	213.8
	1 wt% Pr-CeO_2	374.4	317.6
	5 wt% Pr-CeO_2	400.6	293.4

Table S3. H_2 uptake (µmol $g_{cat.}^{-1}$) of the CeO_2-ZrO_2 solid solutions, precious metals (PM) promoted CeO_2, and rare earth metals (REM) promoted CeO_2 catalysts used in long-term DMC synthesis. For the PM and REM promoted materials only the contribution for the surface reduction has been included.

Material type		**H_2 consumption in µmol $g_{cat.}^{-1}$**
CeO_2-ZrO_2 solid solutions	CeO_2	**376** (**surface** + bulk = 733)
	CeO_2-ZrO_2 [78-22]	401
	CeO_2-ZrO_2 [50-50]	532
	CeO_2-ZrO_2 [25-75]	408
	ZrO_2	no reduction
Precious metals (PM) – CeO_2	1 wt% Rh-CeO_2	355
	1 wt% Ru-CeO_2	274
	1 wt% Pd-CeO_2	533
Rare earth metals (REM) – CeO_2	0.25 wt% La-CeO_2	372
	1 wt% La-CeO_2	434
	5 wt% La-CeO_2	472
	0.25 wt% Gd-CeO_2	406
	1 wt% Gd-CeO_2	479
	5 wt% Gd-CeO_2	369
	0.25 wt% Pr-CeO_2	404
	1 wt% Pr-CeO_2	420
	5 wt% Pr-CeO_2	371

References

1. Tomishige, K.; Furusawa, Y.; Ikeda, Y.; Asadullah, M.; Fujimoto, K., *Catal. Lett.* **2001,** *76*, 71-74.
2. Tomishige, K.; Kunimori, K., *Appl. Catal. A-Gen.* **2002,** *237*, 103–109.
3. Hofmann, H. J.; Brandner, A.; Claus, P., *Chem. Eng. Technol.* **2012,** *35*, 2140–2146.
4. Lee, H. J.; Park, S.; Song, I. K.; Jung, J. C., *Catal. Lett.* **2011,** *141*, 531-537.
5. Lee, H. J.; Joe, W.; Song, I. K., *Korean J. Chem. Eng.* **2012,** *29*, 317-322.
6. Wang, M.; Wang, H.; Zhao, N.; Wei, W.; Sun, Y., *Catal. Commun.* **2006,** *7*, 6–10.
7. Wang, M.; Zhao, N.; Wei, W.; Sun, Y., *Ind. Eng. Chem. Res.* **2005,** *44*, 7596–7599.
8. Joe, W.; Lee, H. J.; Hong, U. G.; Ahn, Y. S.; Song, C. J.; Kwon, B. J.; Song, I. K., *J. Ind. Eng. Chem.* **2012,** *18*, 1018–1022.
9. Joe, W.; Lee, H. J.; Hong, U. G.; Ahn, Y. S.; Song, C. J.; Kwon, B. J.; Song, I. K., *J. Ind. Eng. Chem.* **2012,** *18*, 1730–1735.
10. Sergent, N.; Lamonier, J.-F.; Aboukaïs, A., *Chem. Mater.* **2000,** *12*, 3830–3835.
11. Tanabe, K., *Mater. Chem. Phys.* **1985,** *13*, 347-364.
12. Yamaguchi, T., *Sekiyu Gakkaishi* **1993,** *36*, 250-267.
13. Tanabe, K.; Yamaguchi, T., *Catal. Today* **1994,** *20*, 185-197.
14. Khaodee, W.; Jongsomjit, B.; Assabumrungrat, S.; Praserthdama, P.; Goto, S., *Catal. Commun.* **2007,** *8*, 548–556.
15. Prymak, I.; Kalevaru, V. N.; Wohlrab, S.; Martin, A., *Catal. Sci. Technol.* **2015,** *5*, 2322-2331.
16. Fornasiero, P.; Dimonte, R.; Rao, G. R.; Kaspar, J.; Meriani, S.; Trovarelli, A.; Graziani, M., *J. Catal.* **1995,** *151*, 168-177.
17. Murota, T.; Hasegawa, T.; Aozasa, S.; Matsui, H.; Motoyama, M., *J Alloy. Compd.* **1993,** *193*, 298-299.